Defining the Characteristics of Type I Interferon Stimulated Genes: Insight from Expression Data and Machine Learning

Haiting Chai[1], Quan Gu[1], Joseph Hughes[1,*], David L. Robertson[1,*]

[1]MRC-University of Glasgow Centre for Virus Research, Glasgow, United Kingdom

*Corresponding authors

E-mail: david.l.robertson@glasgow.ac.uk, joseph.hughes@glasgow.ac.uk

Abstract

A virus-infected cell triggers a signalling cascade resulting in the secretion of interferons (IFNs), which in turn induce the up-regulation of IFN-stimulated genes (ISGs) that play an important role in the inhibition of the viral infection and the return to cellular homeostasis. Here, we conduct detailed analyses on 7443 features relating to evolutionary conservation, nucleotide composition, gene expression, amino acid composition, and network properties to elucidate factors associated with the stimulation of genes in response to type I IFNs. Our results show that ISGs are less evolutionary conserved than genes that are not significantly stimulated in IFN experiments (non-ISGs). ISGs show significant depletion of GC-content in the coding region of their canonical transcripts, which leads to under-representation in the nucleotide compositions. Differences between ISGs and non-ISGs are also reflected in the properties of their coded amino acid sequence compositions. Network analyses show that ISG products tend to be involved in key paths but are away from hubs or bottlenecks of the human protein-protein interaction (PPI) network. Our analyses also show that interferon-repressed human genes (IRGs), which are down-regulated in the presence of IFNs, can have similar properties to ISGs, thus leading to false positives in ISG predictions. Based on these analyses, we design a machine learning framework integrating the usage of support vector machine (SVM) and feature selection algorithms. The ISG prediction achieves an area under the receiver operating characteristic curve (AUC) of 0.7455 and demonstrates the similarity between ISGs triggered by type I and III IFNs. Our machine learning model predicts a number of genes as potential ISGs that so far have shown no significant differential expression when stimulated with IFN in the cell types and tissue types compiled in the available IFN-related databases. A webserver implementing our method is accessible at http://isgpre.cvr.gla.ac.uk/.

Author summary

Interferons (IFNs) are signalling proteins secreted from host cells. IFN-triggered signalling activates the host immune system in response to intra-cellular infection. It results in the stimulation of many genes that have anti-pathogen roles in host defenses. Interferon-stimulated genes (ISGs) have unique properties that make them different from those not significantly up-regulated in response to IFNs (non-ISGs). We find the down-regulated interferon-repressed genes (IRGs) have some shared properties with ISGs. This increases the difficulty of distinguishing ISGs from non-ISGs. The use of machine learning is a sensible strategy to provide high throughput classifications of putative ISGs, for investigation with *in vivo* or *in vitro* experiments. Machine learning can also be applied to human genes

for which there are insufficient expression levels before and after IFN treatment in various experiments. Additionally, the interferon type has some impact on ISG predictability. We expect that our study will provide new insight into better understanding the inherent characteristics of human genes that are related to response in the presence of IFNs.

Introduction

Interferons (IFNs) are a family of cytokines originally defined for their capacity to interfere with viral replication. They are secreted from host cells after an infection by pathogens such as bacteria or viruses to trigger the innate immune response with the aim of inhibiting viral spread by 'warning' uninfected cells [1]. The response induced by IFNs is usually fast and feedforward, especially to synthesize new IFNs, which guarantees a full response even if the initial activation is limited [2]. In humans, seven IFNs have been discovered and grouped into three types based on distinct receptors on the cell surface, i.e., IFN-α receptor (IFNAR), IFN-γ receptor (IFNGR), and IFN-λ receptor 1 (IFNLR1)/interleukin-10 receptor 2 (IL-10R2) in the signalling cascade (**Fig 1**) [3]. Type I and III IFNs both help to regulate and activate host immune response, but the function of the latter group is less intense than the former [4-6]. Type II IFNs are also anti-pathogen, immunomodulatory, and proinflammatory but focus on establishing cell immunity [5, 7, 8]. All three types of IFNs are capable of activating the Janus kinase/signal transducer and activator of transcription (JAK-STAT) pathway and inducing the transcriptional up-regulation of approximately 10% of human genes that prime cells for stronger pathogen detections and defenses [9-11]. Henceforth, these up-regulated human genes are referred to as IFN-stimulated genes (ISGs). They play an important role in the establishment of cellular antiviral state, the inhibition of viral infection and the return to cellular homeostasis [8-10, 12]. For example, the ectopic expression of ISG: heparinase (HPSE) can inhibits the attachment of multiple viruses [13, 14]; interferon induced transmembrane proteins (IFITM) can impair the entry of multiple viruses and traffic viral particles to degradative lysosomes [15, 16]; MX dynamin like GTPase proteins (MX) can effectively block early steps of multiple viral replication cycles [17]. The qualitative nature of ISGs is determined by the balance between the activation of signal transducers and activators of transcription (STAT) and IFN-stimulated gene factor 3 complex (ISGF3)/IFN-γ activation factor (GAF) (**Fig 1**) [18]. Abnormality in the IFN-signalling cascade, e.g., the absence of signal transducer and activator of transcription 1 (STAT1) will lead to the failure of activating ISGs, making the host cell highly susceptible to virus infections [19].

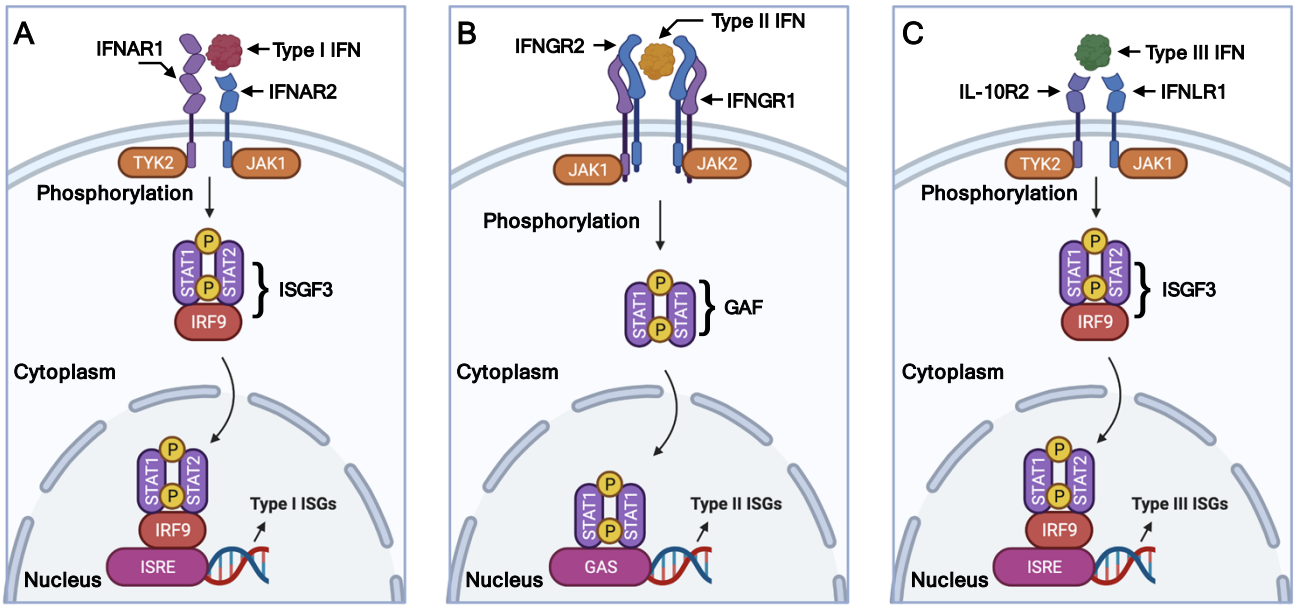

Fig 1. Illustration of signalling cascade triggered by different IFNs. In (A), type I IFN signals through IFNAR, Janus kinase 1 (JAK1), tyrosine kinase 2 (TYK2), STAT, and IFN-regulatory factor 9 (IRF9) to form ISGF3, and then bind to IFN-stimulated response elements (ISRE) to induce the expression of type I ISGs. In (B), type II IFN signals through IFNGR, JAK1 and JAK2 to form GAF and then bind to gamma-activated sequence promoter elements (GAS) to induce the expression of type II ISGs. In (C), type III IFN signals through IFNLR1, IL-10R2, JAK1, TYK2, STAT, and IRF9 to form ISGF3, and then bind to ISRE to induce the expression of type III ISGs. Figure created using the BioRender (https://biorender.com/). Abbreviations: IFNs, interferons; IFNAR, IFN-α receptor; ISGF3, IFN-stimulated gene factor 3 complex; ISGs, interferon-stimulated human genes; IFNGR, IFN-γ receptor; GAF, IFN-γ activation factor; IFNLR1, IFN-λ receptor 1; IL-10R2, interleukin-10 receptor 2; STAT, signal transducers and activators of transcription.

Most research on ISGs has focused on elucidating the role of ISGs in antiviral activities or discovering new ISGs within or across species [8-10, 15, 20, 21]. The identification of ISGs can be achieved via various approaches. Associating gene expression with suppression of viral infection is a good strategy to identify ISGs with obvious antiviral performance, exemplified by the influenza inhibitor, MX dynamin like GTPase 1 (MX1), and the human immunodeficiency virus 1 inhibitor, MX dynamin like GTPase 2 (MX2) [17]. CRISPR screening is a loss-of-function experimental approach to identify ISGs required for IFN-mediated inhibition to viruses, e.g., it enabled the discovery of tripartite motif containing 5 (TRIM5), MX2 and bone marrow stromal cell antigen 2 (BST2) [22]. Monitoring the ectopic expression of ISGs is an instrumental way to find some ISGs that are individually sufficient for viral suppression, e.g. interferon stimulated exonuclease gene 20 (ISG20)

and ISG15 ubiquitin like modifier (ISG15) [23]. Using fold change-based criterion to measure whether a target human gene is induced by IFN signalling now has become a well-accepted idea, but the upregulation cut-off may vary in different studies [21, 24, 25]. The online database, Interferome (http://www.interferome.org), provides an excellent resource by compiling *in vivo* and *in vitro* gene expression profiles in the context of IFN stimulation [21]. The Orthologous Clusters of Interferon-stimulated Genes (OCISG, http://isg.data.cvr.ac.uk) provides an evolutionary comparative approach of genes differentially expressed in the type I IFN system for ten different species [8]. The later study employed a standardised experimental protocol of fibroblast cells stimulated by type I IFN.

Although these studies contribute to a better understanding and detection of ISGs, the knowledge they compiled was limited to a specific IFN type in specific organs, tissues or cells [2]. Despite some well-investigated ISGs, the majority of classified ISGs have limitedly expression following IFN stimulations [8, 21], which means the difference between ISGs and those human genes not significantly up-regulated in the presence of IFNs (non-ISGs) may not be obvious especially when being assessed more generally. It should also be noted that, within non-ISGs, there are a group of genes down-regulated during IFN stimulations. Here, we refer to them as interferon-repressed human genes (IRGs) and they constitute another major part of the IFN regulation system [8, 26]. Collectively, the complex nature of the IFN-stimulated system results in knowledge that is far from comprehensive.

Hence, we seek to characterise the properties of ISGs and to determine whether genes can be identified as ISGs using an *in-silico* machine learning approach. We choose experimental data from human fibroblast cells as the baseline and focus on human genes stimulated by the type I IFNs. We construct a refined high-confidence dataset consisting of 620 ISGs and 874 non-ISGs by cross-checking the genes across multiple databases including the OCISG [8], Interferome [21], and Reference Sequence (RefSeq) [27]. The analyses are conducted primarily on our refined data using genome- and proteome-based features that are likely to influence the expression of human genes in the presence of type I IFNs. Then based on the calculated features, we design a machine learning framework with an optimised feature selection strategy for the prediction of putative ISGs in different IFN systems. Finally, we also develop an online webserver that implements our machine learning method at http://isgpre.cvr.gla.ac.uk/.

Methods

Dataset preparation

In this study, we retrieve 2054 ISGs (Log_2(Fold Change)>2), 12379 non-ISGs (Log_2(Fold Change) <1), and 3944 human genes with low expression levels in IFN experiments (ELGs, expression-limited genes with less than 1 count per million reads mapping across the three biological replicates [28, 29]) from the OCISG (http://isg.data.cvr.ac.uk/) [8]. Gene clusters in the OCISG are built by using the Ensembl Compara database [30], which provides a thorough account of gene orthology based on whole genomes available in the Ensembl database [31]. Labels of these human genes are defined based on the fold change (before and after IFN treatments) and a false discovery rate following IFN treatments in human fibroblast cells. We search the collected 18377 entries against the RefSeq database (https://www.ncbi.nlm.nih.gov/refseq/) [27] to decipher features based on appropriate transcripts (canonical) [32] coding for the main functional isoforms of these human genes, obtaining 1315, 7304, and 2217 results for ISGs, non-ISGs and ELGs, respectively. These 10836 human genes are well-annotated by multiple online databases and are used as the background set (i.e., dataset S1) in the analyses.

For the purpose of generating a set of human genes with high confidence of being interferon-up-regulated and non-up-regulated in response to the type I IFNs, we search labelled human genes against the Interferome database (http://www.interferome.org/) [21]. We filter out ISGs without high up-regulation (Log_2(Fold Change) > 1.0) or with obvious down-regulation (Log_2(Fold Change) < -1.0) in the presence of type I IFNs. This procedure guarantees a refined ISGs dataset with strong levels of stimulation induced by type I IFNs and reduces biases driven by IRGs for the analyses and predictions. We filter out non-ISGs showing enhanced expression after type I IFN treatments (Log_2(Fold Change) > 0). The exclusion of these non-ISGs can effectively reduce the risk of involving false negatives in analyses and producing false positives in predictions. As a result, the refined dataset S2 contains 620 ISGs and 874 non-ISGs with relatively high confidence.

The training procedure in the machine learning framework is conducted on a balanced dataset: S2' consisted of 992 randomly selected ISGs and non-ISGs from dataset S2. The remaining human genes in S2 are used for independent testing. Additionally, we also construct another six testing datasets for the purpose of review and assessment. Dataset S3 contains 695 ISGs with low confidence compared to those ISGs in dataset S2. Some of them could be IRGs in the type I IFN system. Dataset S4 contains 1006 IRGs from the human fibroblast cell experiments. Dataset S5, S6, and S7 are constructed based on records for experiments in type I, II, and III IFN systems from the Interferome database [21]. The criterion for an ISG in the latter three datasets is a high level of up-regulation

167 (Log_2(Fold Change) > 1.0) while that for non-ISGs is no up-regulation after IFN treatments (Log_2(Fold
168 Change) < 0). The last testing dataset S8 is derived from our background dataset S1, containing 2217
169 ELGs. A breakdown of the aforementioned eight datasets is shown in **Table 1**. Detailed information
170 of the human genes used in this study is provided in **S1 Data**.
171
172 **Table 1. A breakdown of datasets used in this study.**

Dataset	Brief description	IFN system	ISGs	Non-ISGs	ELGs
S1	Well-annotated human genes	Type I in fibroblast cells	1315	7304	2217
S2	Refined dataset with high confidence	Type I in fibroblast cells	620	874	0
S2'	Training subset of S2	Type I in fibroblast cells	496	496	0
S2''	Testing subset of S2	Type I in fibroblast cells	124	378	0
S3	ISGs with low confidence in S1	Type I in fibroblast cells	695	0	0
S4	IRGs divided from S1	Type I in fibroblast cells	0	1006	0
S5	ISGs from the Interferome database [21]	Type I in all cells	1259	872	0
S6	ISGs from the Interferome database [21]	Type II in all cells	2229	755	0
S7	ISGs from the Interferome database [21]	Type III in all cells	33	1683	0
S8	ELGs divided from S1	Type I in fibroblast cells	0	0	2217

173 **Abbreviations**: ISGs, interferon-stimulated human genes; non-ISGs, human genes not significantly up-regulated by interferons; IRGs,
174 interferon-repressed human genes, ELGs, human genes with limited expression in interferon experiments.
175
176 **Generation of parametric features**
177 We encode 397 parametric features from aspects of evolution, nucleotide composition, transcription,
178 amino acid composition, and network preference. From the perspective of evolution, we use the
179 number of transcripts and open reading frames (ORFs) to reflect alternative splicing diversity and gene
180 polymorphism respectively. Genes with more transcripts and ORFs have higher alternative splicing
181 diversity and polymorphism to produce proteins with similar or different biological functions [33, 34].
182 We use the number of protein-coding exons in the canonical transcripts to reflect the complexity of
183 the alternative splicing [35]. Genes with more protein-coding exons in their canonical transcripts are
184 considered to produce more complex alternative splicing products [36]. Here, duplication and mutation
185 features are measured by the number of within species paralogues and substitutions [37, 38]. These
186 data are collected from the BioMart [31] to assess the selection on protein sequences and mutational
187 processes affecting the human genome [39].
188 From the perspective of nucleotide composition, we calculate the percent of adenine, thymine,
189 cytosine, guanine, and their four-category combinations in the coding region of the canonical transcript.
190 The first category measures the proportion of two different nitrogenous bases out of the implied four

bases, e.g., GC-content. The second category also focuses on the combination of two nucleotides but involves the impact of phosphodiester bonds along the 5' to 3' direction, e.g., CpG-content [40]. The third category calculates the occurrence frequency of 4-mers, e.g., 'CGCG' composition to involve some positional resolution [41]. The last category considers the co-occurrence of some short linear motifs (SLims) in the complementary DNA (SLim_DNAs). From the perspective of transcription, we calculate the usage of 61 coding codons and three stop codons in the coding region of the canonical transcripts. Codon usage biases are observed when there are multiple codons available for coding one specific amino acid. They can affect the dynamics of translation thus regulate the efficiency of translation and even the folding of the proteins [42, 43].

From the perspective of amino acid composition, we calculate the percentage of 20 standard amino acids and their combinations based on their physicochemical properties [44]. Patterns in the amino acid level are considered to have a direct impact on the establishment of biological functions or to reflect the result of strong purifying selection [45]. Based on the chemical properties of the side chain, we group amino acids into seven classes including aliphatic, aromatic, sulfur, hydroxyl, acidic, amide, and basic amino acids. We also group amino acids based on geometric volume, hydropathy, charge status, and polarity, but find some overlaps among these features. For instance, amino acids with basic side chains are all positively charged. Aromatic amino acids all have large geometric volumes (volume > 180 cubic angstroms). Likewise, we also consider the co-occurrence of some SLims at the protein level. These co-occurring SLims in the protein sequence (SLim_AAs) may relate to potential mechanisms regulating the expression of ISGs [46].

When trying to measure the network preference for the gene products, we construct a human protein-protein interaction (PPI) network based on 332,698 experimentally verified interactions (confidence score > 0.63) from the Human Integrated Protein-Protein Interaction rEference database (HIPPIE, http://cbdm-01.zdv.uni-mainz.de/~mschaefer/hippie/) [47]. Nodes and edges of this network are provided at http://isgpre.cvr.gla.ac.uk/. Eight network-based features including the average shortest path, closeness, betweenness, stress, degree, neighbourhood connectivity, clustering coefficient, and topological coefficient are calculated from this network. Isolated nodes or proteins are not included in our network and are assigned zero value for all these eight features. The shortest path measures the average length of the shortest path between a focused node and others in the network. Closeness of a node is defined as the reciprocal of the length of the average shortest path. Proteins with a low value of the shortest paths or closeness are close to the centre of the network. Betweenness reflects the degree of control that one node exerted over the interactions of other nodes in the network [48]. Stress of a node measures the number of shortest paths passing through it. Proteins with a high value of betweenness or stress are close to the bottleneck of the network. Degree of a node counts the number

of edges linked to it while neighbourhood connectivity reflected the average degree of its neighbours. Proteins with high degree or neighbourhood connectivity are close to the hub of the network. They are considered to play an important role in the establishment of the stable structure of the human interactome [49]. Clustering and topological coefficient measure the possibility of a node to form clusters or topological structures with shared neighbours. The former coefficient can be used to identify the modular organisation of metabolic networks [50] while the latter one may be helpful to find out virus mimicry targets [51].

Generation of non-parametric features

In this study, non-parametric features are used to check the occurrence of SLims in the genome and proteome. The SLim_DNAs we constructed in this study contain three to five random nucleotides, producing 708,540 alternative choices. SLim_DNAs with no restrictions on their first or last position are not taken into consideration as their patterns can be expressed in a more concise way. A SLim_DNA will be picked out to encode a binary feature when its occurrence level in the coding region of the canonical ISG transcripts is significantly higher than that for non-ISGs (Pearson's chi-squared test: $p < 0.05$). SLim_AAs are constructed with three to four fixed amino acids separated by putative gaps. The gap can be occupied by at most one random amino acid, producing 1,312,000 alternative choices. Likewise, binary features are prepared for SLim_AAs showing significant enrichment in ISGs products than in non-ISG products (Pearson's chi-squared test: $p < 0.05$). Since there are lots of results rejecting the null-hypothesis, we adopt the Benjamini-Hochberg correction procedure to avoid type I error [52]. Additionally, we also encode two features to check the co-occurrence or absence of multiple SLim_DNAs and SLim_AAs. This co-occurrence status may be a better representation of functional sites composed of short stretches of adjacent nucleobases or amino acids surrounding SLim_DNAs or SLim_AAs[45].

Assessment of associations between feature representation and IFN-triggered stimulations

In this study, we obtain 8619 human genes with expression data from the OCISG [8]. 4111 of them are annotated with a positive Log_2(Fold Change) ranging from 0 to 12.6, which means they are up-regulated after IFN treatments. In order to measure the average level of feature representation (AREP) for genes with similar expression during IFN stimulations, we introduce a 0.1-length sliding-window to divide the data into 126 bins with different Log_2(Fold Change). Here, Pearson's correlation coefficient (PCC) is introduced to test the association between the representation of parametric features and IFN-triggered stimulation (Log_2(Fold Change) > 0). It can be formulated as:

$$PCC(f) = \frac{1}{n-1}\sum_{i=1}^{n}\left(\frac{LFC_i - M_0}{SD_0}\right) \times \left(\frac{AREP_i - M_f}{SD_f}\right) \quad (1)$$

where n is the number of divided parts that equals to 126 in this study; LFC_i and $AREP_i$ are the value of Log_2(Fold Change) and AREP in the i-th part; M_0 and SD_0 are the mean and standard deviation of Log_2(Fold Change), which is set as 6.4 and 3.7 respectively in this study; M_f and SD_f are the mean and standard deviation of 126 AREP that reflect the representation of the considered feature. To make fair comparisons among features with different scales, we normalise them based on the major value of their representations:

$$Norm(f) = \begin{cases} 1, f > UB(f) \\ \dfrac{f - LB(f)}{UB(f) - LB(f)}, \; LB(f) < f < UB(f) \\ 0, f < LB(f) \end{cases} \quad (2)$$

where $LB(f)$ and $UB(f)$ are the lower and upper bound representing the 5th and 95th percentile within representation values for the target feature. The representation of feature is considered to have a stronger positive/negative association with IFN-triggered stimulations if the PCC calculated from the normalised features is closer to 1.0/-1.0 and the p value calculated by the Student t-test is lower than 0.05.

Machine learning and optimisation

In this study, we introduce a machine learning framework for the prediction of ISGs. Firstly, all features are encoded and normalised based on their major representations (**Equation 2**). Then we use an under-sampling procedure to generate a balanced dataset from the main dataset for training and modelling. Support vector machine (SVM) with radial basis function (RBF) [53] is used as the basic classifier, and it maps the normalised feature space to a higher dimension to generate a space plane to better classify the majority of positive and negative samples. Since there are usually lots of noisy data distributed in the feature space, it is necessary to remove disruptive features. This will effectively reduce the dimensionality of the feature space and make it easier for the SVM model to generate a more appropriate classification plane that involved fewer false positives and false negatives. Here, we develop a subtractive iteration algorithm driven by the change of area under the receiver operating characteristic curve (AUC) to filter out disruptive features (**Fig 2**). In each iteration, we traverse the features and remove those that do not improve the AUC of the prediction results. Theoretically, this algorithm can greatly optimise the feature space and remove all disruptive features after multiple iterations. In the testing procedure, we encode the optimum features for testing samples and place them in the optimised feature space. Samples with longer distance to the optimised classification plane

indicate a stronger signal of being ISGs or non-ISGs. They are more likely to get higher probability scores (close to 0 or 1) from the SVM model.

BEGIN

Initialisation: Balanced dataset $S_0 = \{(1, v_1^0), .. (1, v_n^0), (0, v_{n+1}^0) \ldots (0, v_{2n}^0)\}$, dimension of the feature vector D_0, machine learning algorithm A, number of disruptive feature $d_0 = D_0$, and iteration round $i = 0$.

While $d_0 > 0$ (i^{th} iteration):

1) Use five-fold cross validation on dataset S_i, prediction $P_i = A(S_i)$;
2) Evaluate the P_i with the criterion of AUC;
3) Remove one feature from feature vector v^i and generate a temporary dataset T_i;
4) Use five-fold cross validation on dataset T_i, prediction $P'_i = A(T_i)$;
5) Evaluate the P'_i with the criterion of AUC;
6) Repeat 4) and 5) for the traversal of D_i features;
7) Traverse v^i and remove m features helpful to improve AUC of P'_i, $d_i = m$;
8) Update dataset $S_{i+1} = \{(1, v_1^{i+1}), .. (1, v_n^{i+1}), (0, v_{n+1}^{i+1}) \ldots (0, v_{2n}^{i+1})\}$, $D_{i+1} = D_i - m$.

End

Output: dataset S_{i-1} encoded by D_{i-1} features.

END

Fig 2. The pseudo-code of the AUC-driven subtractive iteration algorithm. Abbreviations: AUC, area under the receiver operating characteristic curve.

Performance evaluation

In this study, the prediction results are evaluated with three threshold-dependent criteria, i.e., sensitivity (SN), specificity (SP), and Matthews correlation coefficient (MCC) [54] and two threshold-independent criteria: SN_n and AUC. SN and SP are used to assess the quality of the machine learning model in recognising ISGs and non-ISGs respectively while MCC provides a comprehensive evaluation for both positives and negatives. The number of 'n' in the SN_n criterion is determined based on the number of ISGs used for testing. It is used to measure the upper limit of the prediction model as well as to check the existence of important false positives close to the class of ISGs from the perspective of data expression. Finally, AUC is a widely used criterion to evaluate the prediction ability of a binary classifier system. The group of interest is almost unpredictable in a specific binary classifier system if the AUC of the classifier is close to 0.5.

Results

Evolutionary characteristics of ISGs

In this study, we construct a dataset consisting of 620 ISGs and 874 non-ISGs (dataset S2) from 10836 well-annotated human genes (dataset S1). Human genes in the S1 dataset have higher confidence based

on their records in both the OCISG [8] and Interferome [21] databases. Human genes in both dataset S1 and S2 are evolutionarily unrelated as they are retrieved from the OCISG [8] that compiles clusters of orthologous genes based on whole-genome alignments. However, they may still have inherent characteristics that have resulted in their different expressions in response to the type I IFNs. Here, we explore features relating to polymorphism [34], alternative splicing [35], duplication [37] and mutation [38]. We use the number of ORFs in a human gene to measure its polymorphism. By calculating the average number of ORFs with respect to different Log_2(Fold Change) levels of expression (window size = 0.1) in the presence of IFNs, we find that human genes with higher Log_2(Fold Change) tend to have lower levels of polymorphism (**Fig 3A**). Although low polymorphism seems to be associated with obvious IFN up-regulation, it is not a necessary condition. Compared to the background human genes we include in dataset S1, we find that ISGs tend to have more ORFs, but these differences are not statistically significant (Mann-Whitney U test: $p > 0.05$). We use the number of transcripts to represent the diversity of alternative splicing for a human gene and use the number of protein-coding exons in the canonical transcript to reflect the complexity of the alternative splicing. For these two features, similar negative relationships are observed when Log_2(Fold Change) increases (**Fig 3B & 3C**). These results illustrate that the simpler the alternative splicing is, the higher the IFN upregulation. Particularly, as the lowest value of Log_2(Fold Change) for human genes not differentially expressed only reaches around -0.9. Points placed left of the boundary (x = -0.9) are IRGs. They are generally placed below those with Log_2(Fold Change) around zero, suggesting the three features (number of ORFs, transcripts and exons) are all differentially represented in some IRGs compared to the remaining non-ISGs. This distribution also indicates that some IRGs have similar feature patterns to ISGs, especially to those highly up-regulated after IFN treatments (right part of the scatter plots in **Fig 3**).

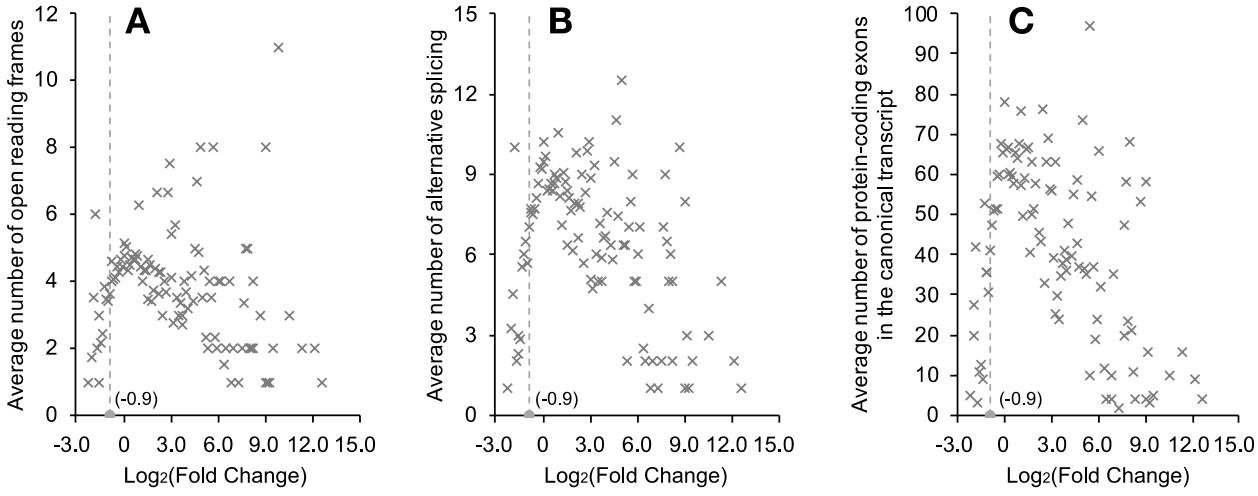

Fig 3. The average representation of features associated with type I IFN stimulations in human fibroblast cells. (A) The number of ORFs as a proxy for gene polymorphism. (B) The number of transcripts as a feature of alternative splicing diversity. (C) The number of protein-coding exons in the canonical transcript as a measurement of the alternative splicing complexity. These three plots are drawn based on the expression data of 8619 human genes with valid fold change in the IFN experiment (**S1 Data**). ELGs are excluded as they have insufficient read coverage to determine a fold change in the IFN experiments. Points in the scatter plot are located based on the average feature representation of genes with similar expression performance in IFN experiments. Abbreviations: IFN, interferon; ORFs, open reading frames; ELGs, human genes with limited expression in interferon experiments.

To determine whether ISGs tend to originate from duplications, we count the number of within human paralogs of each gene (**Fig 4A**). The results show that there are around 22% of singletons in our main dataset, whilst ISGs have 15% and non-ISGs have 26%. The result of a Mann-Whitney U test [55] indicates that the number of paralogs is significantly under-represented in ISGs compared to the background human genes in dataset S1 (M_1 = 10.5, M_2 = 11.5, p = 8.8E-03). We hypothesize that such a difference is mainly caused by the imbalanced distribution of singletons in ISGs and non-ISGs. The differences become smaller when singletons are excluded from the test (M_1 = 12.4, M_2 = 14.6, p > 0.05). Next, we use the number of non-synonymous substitutions per non-synonymous site (dN) and synonymous substitutions per synonymous site (dS) within human paralogues as a measurement of differences in mutational signatures between different classes [56]. As shown in **Fig 4B**, non-synonymous substitutions are more frequently observed in ISGs than in background human genes (M_1 = 0.62, M_2 = 0.55, p = 4.0E-03). On the other hand, ISGs also have a higher frequency of synonymous substitutions than background human genes (M_1 = 37.7, M_2 = 34.6, p = 1.1E-02) (**Fig 4C**) but the difference is not as obvious as for non-synonymous substitutions. The distribution of dN/dS ratios within human paralogues (**Fig 4D**) indicates that most human genes are constrained by natural selection but ISGs, in general, tend to be less conserved (M_1 = 0.036, M_2 = 0.045, p = 8.3E-03). When eliminating the influence of duplication events, ISGs are still less conserved than non-ISGs but the difference in the dN/dS ratio is not significant (M_1 = 0.053, M_2 = 0.031, p > 0.05).

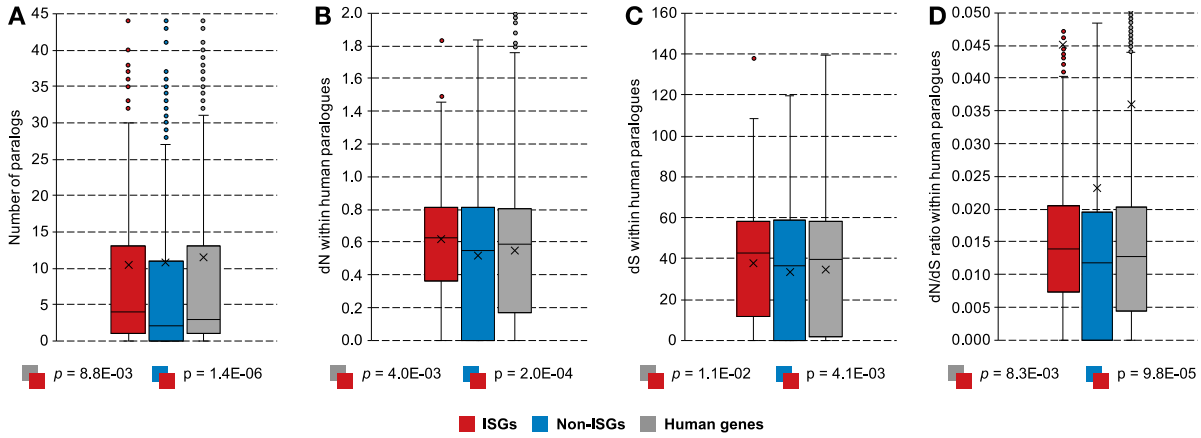

Fig 4. Differences in the evolutionary constraints of human genes. (A) Paralogues within *Homo sapiens*. (B) Non-synonymous substitutions within human paralogues. (C) Synonymous substitutions within human paralogues. (D) dN/dS ratios within human paralogues. Here, ISGs and non-ISGs are taken from dataset S2 while the background human genes are from dataset S1. Mann-Whitney U tests are applied for the hypothesis testing between the feature distribution of different classes. Boxes in the plot represent the major distribution of values (from the first to the third quartile); outliers are added for values higher than two-fold of the third quartile; cross symbol marks the position of the average value including the outliers; upper and lower whiskers show the maximum and minimum values excluding the outliers. Abbreviations: ISGs, interferon upregulated genes; non-ISGs, human genes not significantly up-regulated by interferons; dN, non-synonymous substitutions per non-synonymous site; dS, synonymous substitutions per synonymous site.

Differences in the coding region of the canonical transcripts

Compared to general profile features (e.g., number of ORFs), the sequences themselves provide more direct mapping to the protein function and structure [57]. Here, we encoded 344 parametric features and 7026 non-parametric features from complementary DNA (cDNA) of the canonical transcript to explore features specific to ISGs. We divide the parametric features into four categories and compare their representations among different classes of human genes, i.e., ISGs, non-ISGs, and the background human genes (**Fig 5**). Firstly, guanine and cytosine are both more depleted in ISGs than non-ISGs, leading to an under-representation of GC-content in ISGs (Mann-Whitney U test: M_1 = 52%, M_2 = 55%, p = 2.3E-11). This attribute is antithetical to the GC-biased gene conversion (gBGC), making ISGs less stable with weak evolutionary conservation (**Fig 4**) [58]. Additionally, the under-representation of GC-content also influences the representation of other dinucleotide features. Among all dinucleotide depletions in ISGs, CpG composition is ranked the first followed by GpG and GpC composition (p = 2.9E-14, 4.9E-13 and 1.2E-10, respectively). In turn, adenine and thymine-related

dinucleotide compositions, exemplified by ApT and TpA are more enriched in ISGs than non-ISGs (p = 8.0E-10 and 8.5E-10, respectively).

Next, we compare the usage of 64 different codons in the third category as their frequencies influence transcription efficiency [43]. Differences between ISGs and background human genes are observed in codons for 11 amino acids including leucine (L), isoleucine (I), valine (V), serine (S), threonine (T), alanine (A), glutamine (Q), lysine (K), glutamic acid (E), arginine (R), and glycine (G). The most significant difference was observed in the usage of codon 'AGA'. Among all arginine-targeted alternative codons, codon 'AGA' is usually favoured, and its usage reaches an estimated 25% in ISGs, but reduces to 22% in the background human genes and is even significantly lower in non-ISGs, at 18% (p = 1.4E-05 and 1.9E-13, respectively). On the other hand, compared to background human genes, the codon 'CAG' coding for amino acid 'Q' is the most under-represented in ISGs. It is less favoured by ISGs than non-ISGs (M_1 = 72%, M_2 = 78%, p = 7.3E-13) although it dominates in coding patterns. As for the three stop codons, comparing with background human genes, the usage of the ochre stop codon, i.e., 'TAA' is over-represented in ISGs (M_1 = 28%, M_2 = 33%, p = 9.7E-03). In this category of codon usage, the features that have different frequencies between ISGs and background human genes became more discriminating when comparing ISGs with non-ISGs. Significant differences in codon usages between ISGs and non-ISGs are widely observed except for methionine (M) and tryptophan (W). Hence, although we find a limited number of codon usage features showing significant differences between ISGs and the background human genes, the codon usage features are useful for discriminating ISGs from non-ISGs.

In the last category, we calculate the occurrence frequency of 256 nucleotide 4-mers to add some positional resolution for finding and comparing interesting organisational structures [41]. Among the 256 4-mers, we find 46 of them are differentially represented between ISGs and background human genes (**S2 Data**). Most of these 4-mers are over-represented by ISGs except two with the pattern 'TAAA' and 'CGCG'. Interestingly, the feature of 'TAAA' composition becomes a positive factor when comparing ISGs and non-ISGs (M_1 = 4.1%, M_2 = 3.7%, p = 4.1E-06), suggesting it may be a good feature to ascertain potential or incorrectly labelled ISGs. We find six nucleotide 4-mers: 'ACCC', 'AGTC', 'AGTG', 'TGCT', 'GACC', and 'GTGC' are over-represented in ISGs when compared to background human genes but are not differentially represented when comparing ISGs with non-ISGs. Thus, these six features may be inherently biased for some unknown reasons and are not powerful enough to distinguish ISGs from non-ISGs. In addition to the aforementioned 40 features that are over-represented in ISGs compared to background human genes, we find a further 39 features nucleotide 4-mers differentially represented between ISGs and non-ISGs (**S2 Data**).

To check the effect of these aforementioned 343 features on the level of stimulation in the IFN system (Log_2(Fold Change) > 0), we calculate the PCC for the normalised features (**Equation 2**) and find 106 features are positively related to the increase of fold change, and 34 features are suppressed when human gene are more up-regulated (Student t-test: $p < 0.05$) (**S3 Data**). ApA composition shows the most obvious positive correlation with stimulation level (PCC = 0.464, p = 8.8E-06) while negative association between the representation of 4-mer 'CGCG' and IFN-induced up-regulation is the most significant (PCC = -0.593, p = 3.2E-09). Human genes with higher up-regulation in the presence of IFNs contain more codons 'CAA' rather than 'CAG' for coding amino acid 'Q'. The depletion of GC-content, especially cytosine content, promotes the suppression of many nucleotide compositions in the cDNA, e.g. CpG composition.

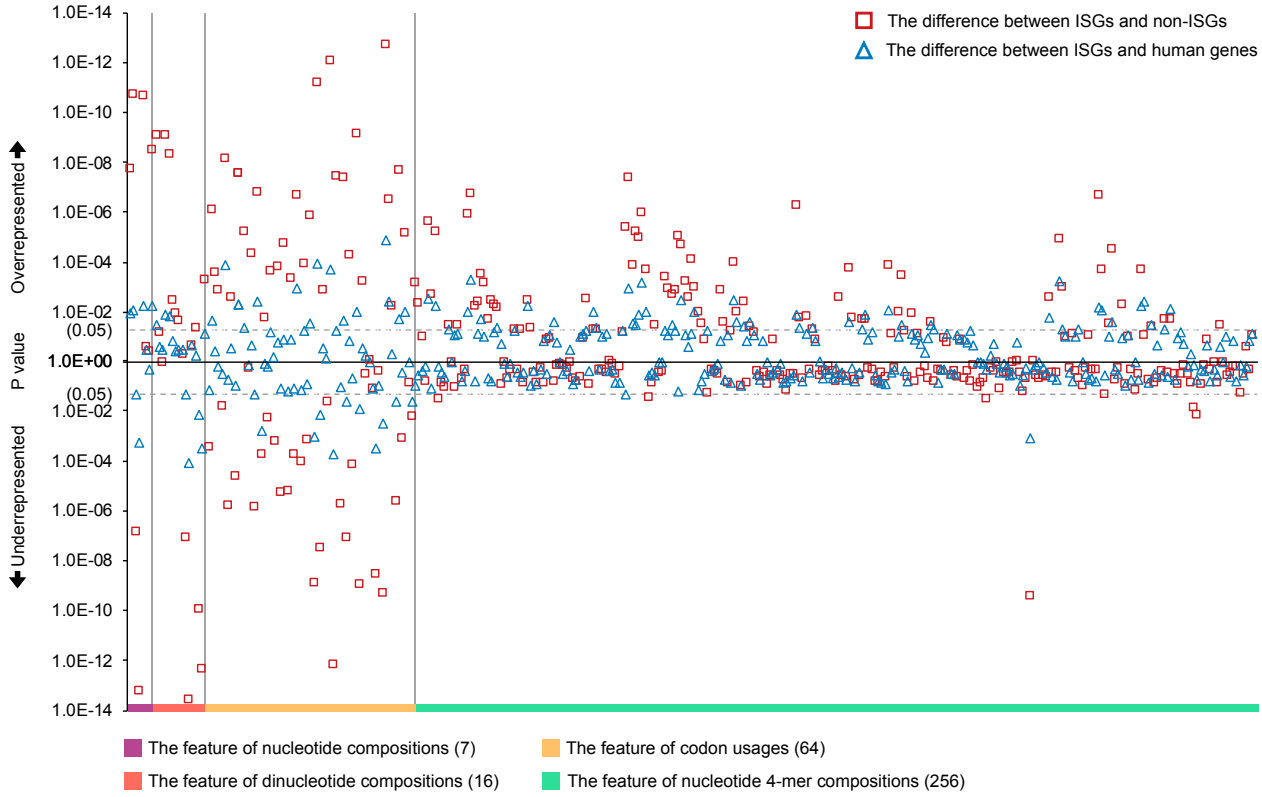

Fig 5. Differences in the representation of parametric features encoded from coding regions of the canonical transcript. Mann-Whitney U tests are applied for hypothesis testing and the results were provided in the **S2 Data**. Here, ISGs and non-ISGs are taken from dataset S2 while the background human genes are from dataset S1. Abbreviations: ISGs, interferon upregulated genes; non-ISGs, human genes not significantly up-regulated by interferons.

To find conserved sequence patterns related to gene regulations [59], we check the existence of 2940, 44100 and 661500 short linear nucleotide motifs (SLim_DNAs) consisting of three to five consecutive nucleobases in the group of ISGs and non-ISGs. By using a positive 5% difference in the occurrence frequency as cut-off threshold, we find 7884 SLim_DNAs with a maximum difference in representation around 15%. After using Pearson's chi-squared tests and Benjamini-Hochberg correction to avoid type I error in multiple hypotheses [52], 7025 SLim_DNAs remain with an adjusted p-value lower than 0.01 (**S4 Data**), hereon referred to as flagged SLim_DNAs. Here, the differentially represented 7025 SLim_DNAs are ranked according to the adjusted p-value. As shown in **Fig 6A**, dinucleotide 'TpA' dominates in the top 10, top 100, top 1000, and all differentially represented SLim_DNAs even if TpA representation is suppressed in the cDNA of genes' canonical transcripts compared to other dinucleotides. Dinucleotide 'ApT' and 'ApA' are also frequently observed in the flagged SLim_DNAs but their occurrences do not show significant difference in the top 100 SLim_DNAs (Pearson's chi-squared test: $p > 0.05$). GC-related dinucleotides, e.g., 'CpC', 'GpC' and 'GpG' are rarely observed in the flagged SLim_DNAs especially in the top 10 or top 100. In view of these, we hypothesize that the differential representation of nucleotide compositions influences and reflects on the pattern of SLim_DNAs in ISGs. By checking the co-occurrence status of the flagged SLim_DNAs, we find these sequence patterns have a cumulative effect in distinguishing ISGs from non-ISGs especially when the number of cooccurring SLim_DNAs reaches around 5320 (Pearson's chi-squared test: $p = 7.9E-13$, **Fig 6B**). There are eight (~1.3%) ISGs in the refined set, i.e., dataset S2 containing all the flagged 7025 SLim_DNAs. Their up-regulation after IFN treatment are generally low with a fold change fluctuating around 2.2. Although some genes such as desmoplakin (DSP) are clearly highly up-regulated in endothelial cells isolated from human umbilical cord veins after both IFN-α (fold change = 11.1) and IFN-β (fold change = 13.7) treatments. We also find some non-ISGs and ELGs containing the flagged SLim_DNAs, e.g., hemicentin 1 (HMCN1) and tudor domain containing 6 (TDRD6), but their frequencies are lower than that in ISGs. Although there is an obvious imbalance between the number of ISGs and non-ISGs in the human genome [9-11], the curve for the background human genes in **Fig 6B** is still closer to that for ISGs rather than that for non-ISGs. It suggests that some genetic patterns are widely represented in the coding region of human genes, making them potentially up-regulated in the IFN system.

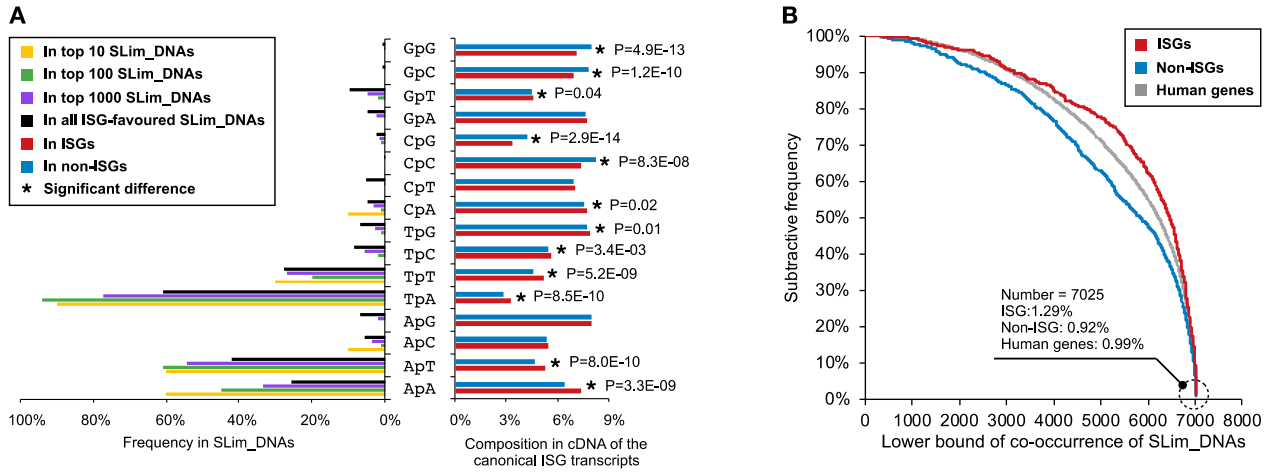

Fig 6. The pattern of SLim_DNAs in the coding region of the canonical transcripts. (A) Influence of dinucleotide compositions on the flagged SLim_DNAs. (B) The co-occurrence status of SLim_DNAs in different human genes. Ranks in (A) are generated based on the adjust p value given by Pearson's chi-squared tests after Benjamini-Hochberg correction procedure. Detailed results of the hypothesis tests are provided in **S4 Data**. Here, ISGs and non-ISGs are taken from dataset S2 while the background human genes are from dataset S1. Abbreviations: ISGs, interferon-stimulated genes; non-ISGs, human genes not significantly up-regulated by interferons; SLim_DNAs, short linear nucleotide motifs; cDNA, complementary DNA.

Differences in the protein sequence

We use the protein sequences generated by the canonical transcript to extract features at the proteomic level. In addition to the basic composition of 20 standard amino acids, we consider 17 additional features related to physicochemical (e.g., hydropathy and polarity) or geometric properties (e.g., volume) [60, 61]. We find several amino acids that are either enriched or depleted in ISG products compared to background human proteins, which are produced by genes in dataset S1 (**Fig 7**). The differences are even more marked between protein products of ISGs and non-ISGs, highlighting some differences that are not observed when comparing ISG products to the background human proteins (e.g., isoleucine composition). The differences observed in the amino acid compositions are at least in part associated with the patterns previously observed in features encoded from genetic coding regions. For example, asparagine (N) shows significant over-representation in ISG products compared to non-ISG products or background human proteins (Mann-Whitney U test: p = 2.8E-12 and 1.2E-03, respectively). This is expected as there are only two codons, i.e., 'AAT' and 'AAC' coding for amino acid 'N', and dinucleotide 'ApA' shows a remarkable enrichment in the coding region of ISGs. A similar explanation can be given for the relationship between the deficiency of GpG content and amino

494 acid 'G'. The translation of amino acid 'K' is also influenced by ApA composition but is not significant
495 due to the mild representation of dinucleotide 'ApG' in the genetic coding region. Additionally, as
496 previously mentioned, ISGs show a significant depletion in the CpG content, and consequently, the
497 amino acid 'A' and 'R' in ISG products are significantly under-represented. Cysteine (C) is not
498 frequently observed in human proteins but still shows a relatively significant enrichment in ISG
499 products (M_1 = 2.3%, M_2 = 2.5%, p = 1.8E-03).
500 When focusing on the composition of amino acids grouped by physicochemical or geometric
501 properties, we also find some features differentially represented between ISG products and background
502 human proteins. The result shows that hydroxyl (amino acid 'S' and 'T'), amide (amino acid 'N' and
503 'Q'), or sulfur amino acids (amino acid 'C' and 'M') are more abundant in ISG products compared to
504 the background human proteins (Mann-Whitney U test: p = 0.04, 1.0E-03 and 0.02, respectively).
505 Small amino acids (amino acid 'N', 'C', 'T', aspartic acid (D) and proline (P), the volume ranges from
506 108.5 to 116.1 cubic angstroms) are more frequently observed in ISG products than in background
507 human proteins (M_1 = 22.1%, M_2 = 21.7%, p = 0.02). The differences become more marked when
508 comparing the representation of these features between ISG and non-ISG products. For example,
509 features relating to chemical properties of the side chain (e.g., aliphatic), charge status and geometric
510 volume show differences between proteins produced by ISGs and non-ISGs. Some features, e.g.,
511 neutral amino acids that include amino acid 'G', 'P', 'S', 'T', histidine (H) and tyrosine (Y) are not
512 differentially represented between ISG and non-ISG products, but they show obvious association with
513 the change of IFN-triggered stimulations (PCC = -0.556, p = 4.1E-08) (**S3 Data**).
514

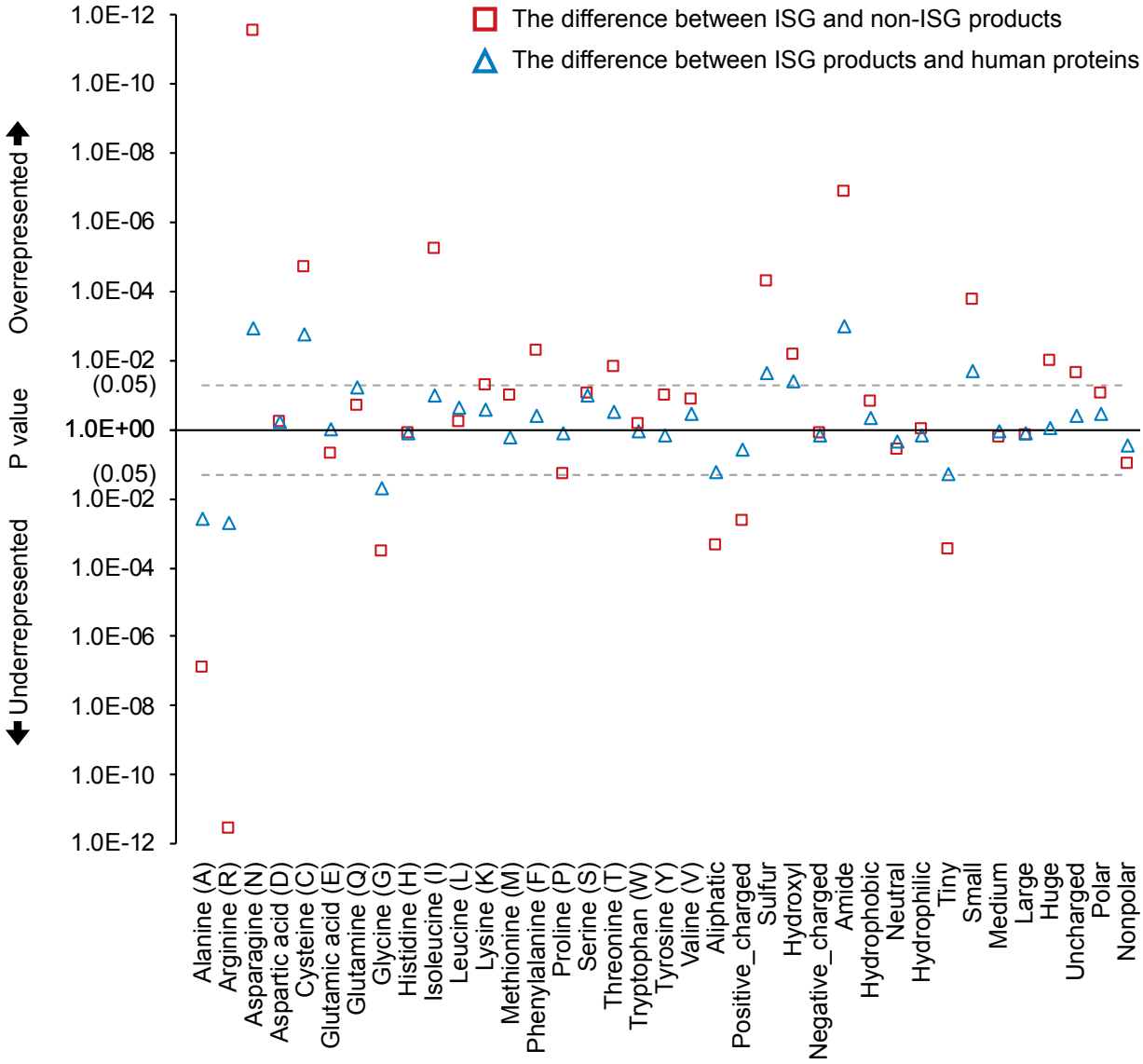

Fig 7. Differences in the representation of parametric features encoded from protein sequences. Mann-Whitney U tests are applied for hypothesis testing and the results were provided in the **S2 Data**. Here, ISGs and non-ISGs are taken from dataset S2 while the background human genes are from dataset S1. Aliphatic group: amino acid 'A', 'G', 'I', 'L', 'P' and 'V'; aromatic/huge group: amino acid 'F', 'W' and 'Y' (volume > 180 cubic angstroms); sulfur group: amino acid 'C' and 'M'; hydroxyl group: amino acid 'S' and 'T'; acidic/negative_charged group: amino acid 'D' and 'E'; amide group: amino acid 'N' and 'Q'; positive_charged group: amino acid 'R', 'H' and 'K'; hydrophobic group: amino acid 'A', 'C', 'I', 'L', 'M', 'F', 'V', and 'W' that participates to the hydrophobic core of the structural domains [44]; neutral group: amino acid 'G', 'H', 'P', 'S', 'T' and 'Y'; hydrophilic group: amino acid 'R', 'N', 'D', 'Q', 'E' and 'K'; Tiny group: amino acid 'G', 'A' and 'S' (volume < 90 cubic angstroms); small group: amino acid 'N', 'D', 'C', 'P' and 'T' (volume ranged from 109 to 116 cubic angstroms); medium group: amino acid 'Q', 'E', 'H' and 'V' (volume ranged within 138 to 153

cubic angstroms); large group: amino acid 'R', 'I', 'L', 'K' and 'M' (volume ranged within 163 to 173 cubic angstroms); uncharged group: the remaining 15 amino acids except electrically charged ones; polar group: amino acid 'R', 'H', 'K', 'D', 'E', 'N', 'Q', 'S', 'T' and 'Y'; nonpolar group: the remaining 10 amino acids except polar ones. Abbreviations: ISG, interferon upregulated genes; non-ISG, human genes not significantly up-regulated by interferons.

We then search the sequence of ISG products against that of non-ISG products to find conserved short linear amino acid motifs (SLim_AAs), which may have resulted from strong purifying selection [45]. As opposed to the analysis on the genetic sequence, we only obtain 19 enriched sequence patterns with a Pearson's chi-squared p value ranging from 1.5E-04 to 0.02 (**Table 2**). These SLim_AAs are greatly influenced by four polar amino acids: 'K', 'N', 'E' and 'S', and one nonpolar amino acid: 'L'. Some of these SLim_AAs, e.g., SLim 'NVT' and 'S-N-E', are clearly over-represented in ISG products compared to background human proteins and can be used as features to differentiate ISGs from background human genes. The third column in **Table 2** also indicates a number of patterns, e.g., SLim 'S-N-T', that are lacking in non-ISG products and hence may be the reason for the lack of up-regulation in the presence of IFNs. Particularly, we noticed that SLim 'KEN' is a destruction motif that can be recognised or targeted by anaphase promoting complex (APC) for polyubiquitination and proteasome-mediated degradation [62, 63]. Results shown in **Fig 8A** illustrate that the co-occurrence of differentially represented SLim_AAs has a cumulative effect in distinguishing ISGs from non-ISGs. This cumulative effect can be achieved with only two random SLim_AAs (Pearson's chi-squared test: p = 4.6E-10). The bias in the co-occurring SLim_AAs in the background human proteins towards a pattern similar to non-ISG products further proves the importance of these 19 SLim_AAs. However, their co-occurrence is not associated with the level of IFN-triggered stimulations (PCC = 0.015, $p > 0.05$) (**Fig 8B**)

Regions that lacked stable structures under normal physiological conditions within proteins are termed intrinsically disordered regions (IDRs). They play an important role in cell signalling [64]. Compared with ordered regions, IDRs are usually more accessible and have multiple binding motifs, which can potentially bind to multiple partners [65]. According to the results calculated by IUPred [66], we find 6721, 10510, and 119071 IDRs (IUpred score no less than 0.5) in proteins produced by ISGs, non-ISGs and background human genes respectively. We hypothesize that enriched SLims widely detected in IDRs may be important for human protein-protein interactions or potentially virus mimicry [51]. For instance, in ISG products, 29 out of 71 SLim 'S-N-T' are observed in IDRs (~40.8%), 14.9% higher than that in non-ISG products (**Table 2**). This difference reflects the importance of SLim 'S-N-T' for target specificity of IFN-induced protein-protein interactions [9] even if it is not

562 statistically significant. By contrast, the conditional frequency of SLim 'S-N-E' is discovered in IDRs
563 of ISG and non-ISG products are almost the same, indicating that SLim 'S-N-E' may have an
564 association with some inherent attributes of ISGs but is less likely to be involved in IFN-induced
565 protein-protein interactions. SLim 'KEN' in IDRs also shows some interesting differences: in non-
566 ISG products, 41.9% of SLim 'KEN' are observed in IDRs, 14.6% higher than that in ISG products,
567 which provides an effective approach to distinguish ISGs from non-ISGs. When SLim 'KEN' is
568 discovered in the ordered region of a protein sequence, statistically, the protein is more likely to be
569 produced by an ISG, but this assumption is reversed if the SLim is located in an IDR (Pearson's chi-
570 squared tests: $p = 0.03$). Despite the relatively low conditional frequency of SLim 'KEN' in the IDRs
571 of ISG products, these SLim_AAs in the IDR are more likely to be functionally active than those
572 falling within ordered globular regions [67].
573

574 **Table 2. Representation of SLims in protein sequences and their IDRs.**

SLims[a]	Frequency in ISG/non-ISG products[b]	Bias based on frequency in human proteins	P value[c]	Conditional frequency in IDRs of ISG/non-ISG products/background human proteins[c,d]	P value[e]
S-N-E	15.2%/8.8%	+47.6%/-14.2%	1.5E-04	39.4%/40.3%/33.4%	0.90
ENE	15.0%/8.8%	+20.9%/-29.0%	2.1E-04	37.6%/42.9%/40.9%	0.49
S-N-T	11.5%/6.2%	+21.9%/-34.2%	2.9E-04	40.8%/25.9%/27.3%	0.08
SVI	15.2%/9.2%	+37.6%/-16.9%	3.6E-04	18.1%/11.3%/15.2%	0.21
L-NL	23.7%/16.4%	+13.2%/-21.9%	4.0E-04	10.2%/11.9%/9.4%	0.65
L-KL	30.8%/22.8%	+18.0%/-12.8%	4.9E-04	12.6%/10.1%/8.7%	0.43
NVT	13.7%/8.5%	+52.1%/-6.1%	1.2E-03	18.8%/21.6%/15.4%	0.66
ISS	20.5%/14.3%	+20.7%/-15.7%	1.7E-03	29.9%/25.6%/23.8%	0.44
LK-K	24.4%/17.7%	+24.5%/-9.3%	1.8E-03	14.6%/20.6%/20.0%	0.16
IK-E	14.2%/9.0%	+34.2%/-14.5%	1.8E-03	26.1%/16.5%/25.8%	0.13
EK-I	15.8%/10.4%	+31.0%/-13.7%	2.0E-03	15.3%/20.9%/16.0%	0.32
K-E-S	16.9%/11.4%	+21.9%/-17.7%	2.4E-03	36.2%/36.0%/39.2%	0.98
LNS	17.7%/12.1%	+21.2%/-17.1%	2.4E-03	20.0%/25.5%/20.5%	0.34
KEN	16.0%/10.6%	+33.5%/-11.0%	2.4E-03	27.3%/41.9%/34.8%	0.03
L-N-L	22.6%/17.5%	+14.3%/-11.4%	1.5E-02	10.7%/11.8%/9.5%	0.78
K-E-L	25.8%/20.5%	+25.7%/-0.3%	1.5E-02	18.8%/17.9%/18.7%	0.84
KLL	27.1%/21.9%	+9.9%/-11.4%	1.9E-02	11.3%/8.4%/9.9%	0.35
LKE	29.8%/24.5%	+18.2%/-3.0%	2.1E-02	19.5%/24.8%/20.1%	0.20
LK-L	33.2%/27.7%	+15.0%/-4.2%	2.1E-02	7.8%/12.4%/10.0%	0.11

575 [a]*the dash symbol in SLims indicates one position occupied by a standard amino acid;* [b]*here, ISGs and non-ISGs are taken from dataset*
576 *S2 while the background human genes use samples in dataset S1;* [c]*p values in this column use Pearson's chi-squared tests to measure*
577 *the difference of SLim occurrences in ISG and non-ISG products;* [d]*frequencies in this column are calculated based on a condition that*

corresponding SLims are observed in the protein sequence; [e]p values in this column use Pearson's chi-squared tests to measure the difference of SLim occurrences in IDRs of ISG and non-ISG products.

Abbreviations: SLims, short linear motifs; ISGs, interferon-stimulated human genes; non-ISGs, human genes not significantly up-regulated by interferons; IDRs, intrinsically disordered regions.

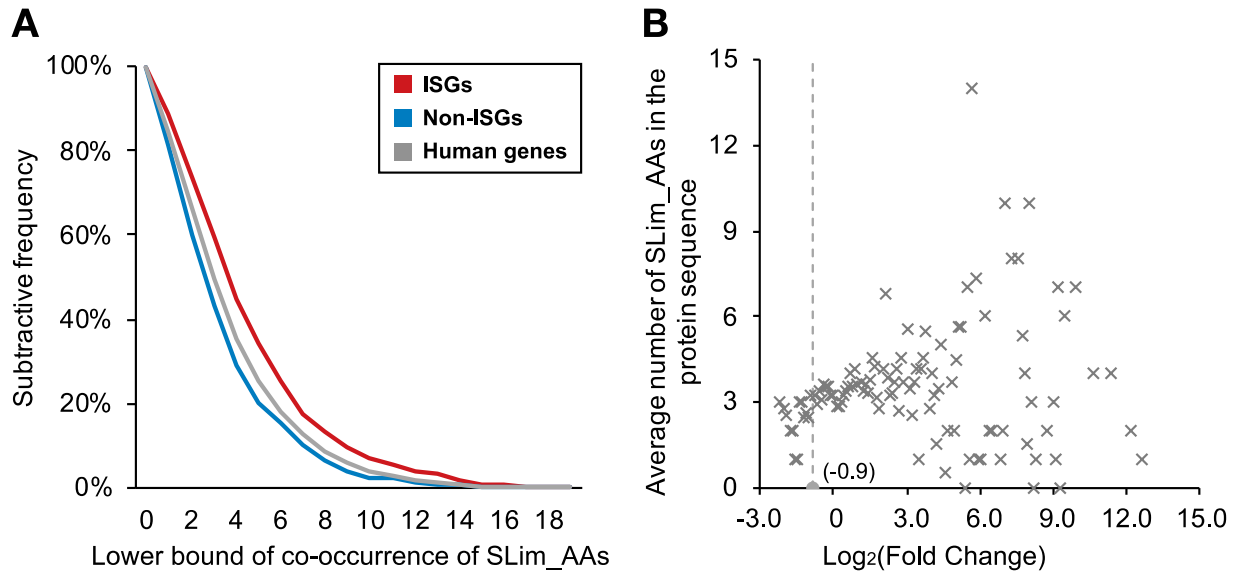

Fig 8. Representation of co-occurred SLim_AAs in our main dataset. (A) The co-occurrence status of SLim_AAs in different classes. (B) Relationship between co-occurrence of the marked SLim_AAs and Log_2(Fold Change) after IFN treatments. Here, ISGs and non-ISGs are taken from dataset S2 while the background human genes are from dataset S1. Points in (B) are located based on the average feature representation of genes with similar expression performance in IFN experiments. Abbreviations: IFN, interferon; ISGs, interferon-stimulated genes; non-ISGs, human genes not significantly up-regulated by interferons; SLim_AAs, short linear amino acid motifs.

Differences in network profiles

We construct a network with 332,698 experimentally verified interactions among 17603 human proteins (confidence score > 0.63) from the HIPPIE database [47]. 10169 out of 10836 human proteins from our background dataset S1 are included in it. Nodes and edges of this network can be downloaded from our webserver at http://isgpre.cvr.gla.ac.uk/. Based on this network, we calculate eight features including the average shortest path, closeness, betweenness, stress, degree, neighbourhood connectivity, clustering coefficient, and topological coefficient. As illustrated in **Fig 9**, ISG products tend to have higher values of betweenness and stress than background human proteins (Mann-Whitney U test: p = 0.01, and 0.03, respectively), which means they are more likely to locate at key paths connecting different nodes of the PPI network. Some ISG products with high values of betweenness

and stress, e.g., tripartite motif containing 25 (TRIM25), can be considered as the shortcut or bottleneck of the network and play important roles in many PPIs including those related to the IFN-triggered immune activities [68, 69]. However, the over-representation of betweenness does not mean ISG products are more likely to be or even be close to bottlenecks in the network compared to background human proteins. Some examples shown in **Table 3** indicate that ISG products are less-connected by top-ranked bottlenecks and hubs in the network than non-ISGs or background human proteins. This conclusion is not influenced by hub/bottleneck protein's performance in the IFN experiments. Comparing proteins produced by ISGs and non-ISGs, we find the former tends to have lower values of clustering coefficient and neighbourhood connectivity (Mann-Whitney U test: $p = 0.04$, and 7.9E-03, respectively), which means that ISG products and the majority of their interacting proteins are less likely to be targeted by lots of proteins. It also supports the finding that ISG products are involved in many shortest paths for nodes but are away from hubs or bottlenecks in the network. To some extents, this location also increases the length of the average shortest paths through ISG products in the network.

When investigating the association between IFN-induced gene stimulation and network attributes of gene products, we only find the feature of neighbourhood connectivity is under-represented as the level of differential expression in the presence of IFN increases (PCC = -0.392, p = 2.2E-04). This suggests that proteins produced by genes that are highly up-regulated in response to IFNs are further away from hubs in the PPI networks.

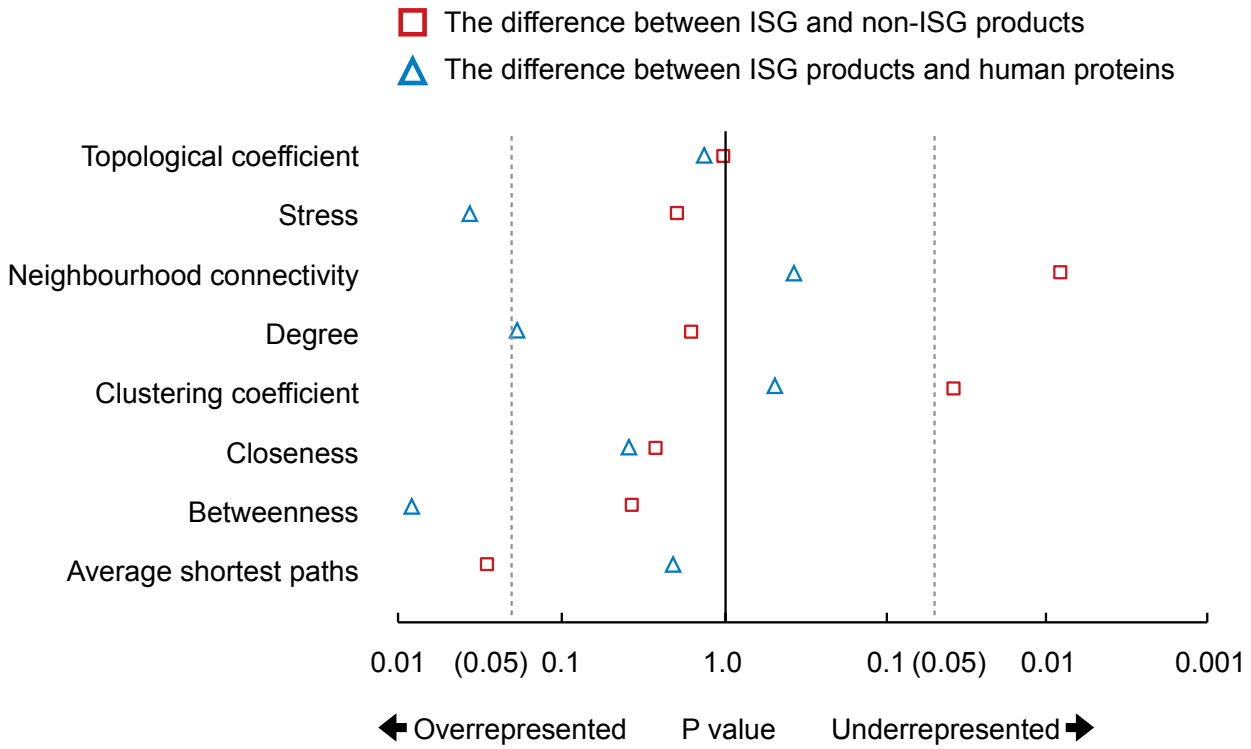

Fig 9. Differential network preferences of proteins coded by different human genes. Mann-Whitney U tests are applied for hypothesis testing and the results were provided in the **S2 Data**. Here, ISGs and non-ISGs are taken from dataset S2 while the background human genes use samples in dataset S1. Abbreviations: ISGs, interferon-stimulated genes; non-ISGs, human genes not significantly up-regulated by interferons.

Table 3. Interaction profiles of human proteins connecting top hubs/bottlenecks of the HIPPIE network.

Human protein	TRIM25	ELAVL1	ESR2	NTRK1	HNRNPL
Gene class	ISG	IRG	Not included in S1[a]		
Degree (hub rank)	2295 (2nd)	1787 (4th)	2500 (1st)	1976 (3rd)	1681 (5th)
Betweenness (bottleneck rank)	0.067 (1st)	0.048 (4th)	0.051 (3rd)	0.026 (5th)	0.052 (2nd)
Difference in interacting partners (ISG products versus non-ISG)[b]	Depleted P = 0.01	P > 0.05	Depleted P = 1.1E-4	Depleted P = 5.5E-3	P > 0.05
Difference in interacting partners (ISG products versus background human proteins)[b]	P > 0.05	P > 0.05	Depleted P = 8.1E-3	Depleted P = 0.03	P > 0.05

[a]*ESR2 and NTRK1 are not included in dataset S1 as their expression data were not compiled in the OCISG, HNRNPL is not included in dataset S1 as its canonical isoform was uncertain when the dataset was constructed;* [b]*differences here are measured via Pearson's chi-squared tests on human proteins interacting with the corresponding hub/bottleneck protein.*

Abbreviations: HIPPIE, Human Integrated Protein-Protein Interaction rEference database; TRIM25, tripartite motif containing 25; ELAVL1, embryonic lethal, abnormal vision like RNA binding protein 1; ESR2, estrogen receptor 2; NTRK1, neurotrophic receptor tyrosine kinase 1; HNRNPL, heterogeneous nuclear ribonucleoprotein L; ISGs, interferon-stimulated human genes; non-ISGs, human genes not significantly stimulated by interferons.

Features highly associated with the level of IFN stimulations

In this study, we encode a total of 397 parametric and 7046 non-parametric features covering the aspects of evolutionary conservation, nucleotide composition, transcription, amino acid composition, and network profiles. In order to find out some key factors that may enhance or suppress the stimulation of human genes in the IFN system, we compare the representation of parametric features of human genes with different Log_2(Fold Change) in experiments on human fibroblast cells stimulated with IFNs (Log_2(Fold Change) > 0). Two features on the co-occurrence of SLims are not taken into consideration here as they are more subjective than the other parametric features and are greatly influenced by the number of focused SLims. Upon the calculation of PCC and the result of hypothesis tests, we find 168 features highly associated with the level of IFN-triggered stimulations (Student t-tests: $p < 0.05$) (**S3 Data**). Among them, 118 features show a positive correlation (**Fig 10**) while the remaining 50 features show a negative correlation (**Fig 11**) with the change of up-regulation in IFN experiments. Three features including the number of ORF, alternative splicing results, and exons in the canonical transcripts are encoded from characteristics of the gene. Two features, i.e., average dN/dS and average dS within human paralogues are encoded based on the sequence alignment results from the Ensembl [31]. 140 and 22 features are encoded from the genetic sequence and proteomic sequence respectively. The last one, i.e., neighbourhood connectivity is obtained from the network profile of a human interactome constructed based on experimentally verified data in the HIPPIE [47].

In the positive group, the feature of 'large' amino acid compositions that includes the composition of five amino acids with geometric volume ranged from 163 to 173 cubic angstroms is ranked the first for having the highest PCC at 0.593 (Student t-test: $p = 2.8E-09$). This feature was not highlighted previously as it did not have a strong signal for discriminating ISGs from non-ISGs (Mann-Whitney U test: $p > 0.05$). Similar phenomena can be found on 87 features (64 positive correlations and 23 negative correlations) such as AG-content, ApG content and previously mentioned neutral amino acid composition. The strongest negative correlation between feature representation and IFN-triggered stimulations is found on the feature of 4-mer 'CGCG' (PCC = -0.593, $p = 3.2E-09$). This feature also shows a differential distribution between ISGs and non-ISGs, which provides useful information to distinguish ISGs from non-ISGs. Similar phenomena can be found on 81 features (54 positive correlations and 27 negative correlations) such as previously mentioned GC-content, CpG content and the usage of codon 'GCG' coding for amino acid 'A'. Collectively, the biased effect on

669 the basic composition of nucleotides influences the correlation between the representation of sequence-
670 based features and IFN-triggered stimulations. Human genes that show over-representation in more
671 features listed in **Fig 10** are expected to be more up-regulated after type-I IFN treatments at least in
672 human fibroblast cells. Meanwhile, the under-representation of features listed in **Fig 11** will also
673 contribute to the level of up-regulation in the IFN experiments.
674

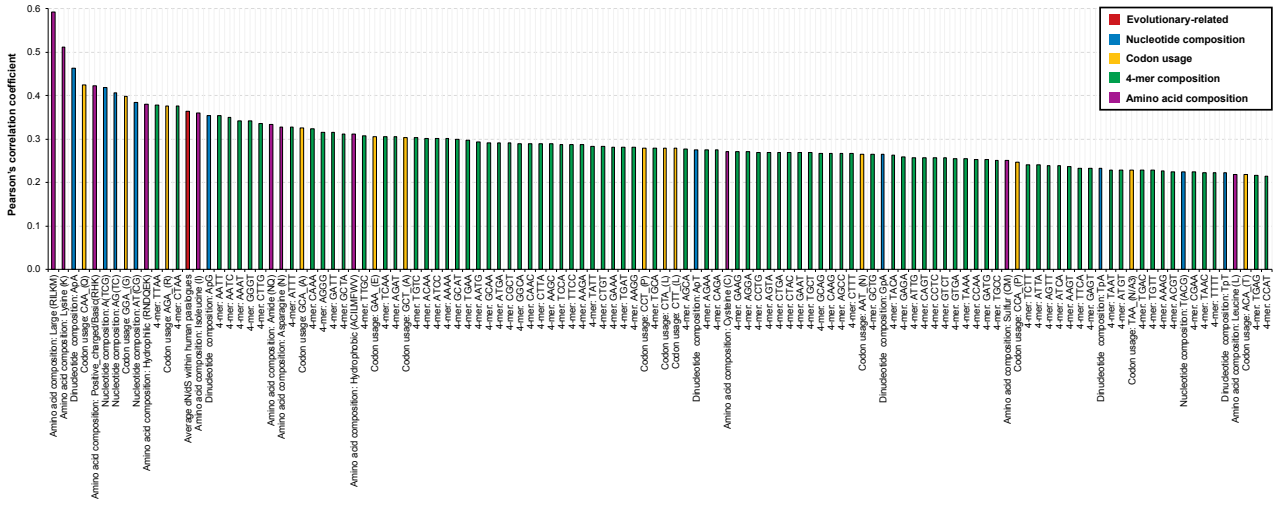

675

676 **Fig 10. 118 features positively associated with higher up-regulation after IFN treatments in**
677 **human fibroblast cells (Student t-tests: p < 0.05).** Detailed results about PCC and hypothesis tests
678 are provided in **S3 Data**. Abbreviations: IFNs, interferons; PCC, Pearson's correlation coefficient; dN,
679 non-synonymous substitutions per non-synonymous site; dS synonymous substitutions per
680 synonymous site.
681

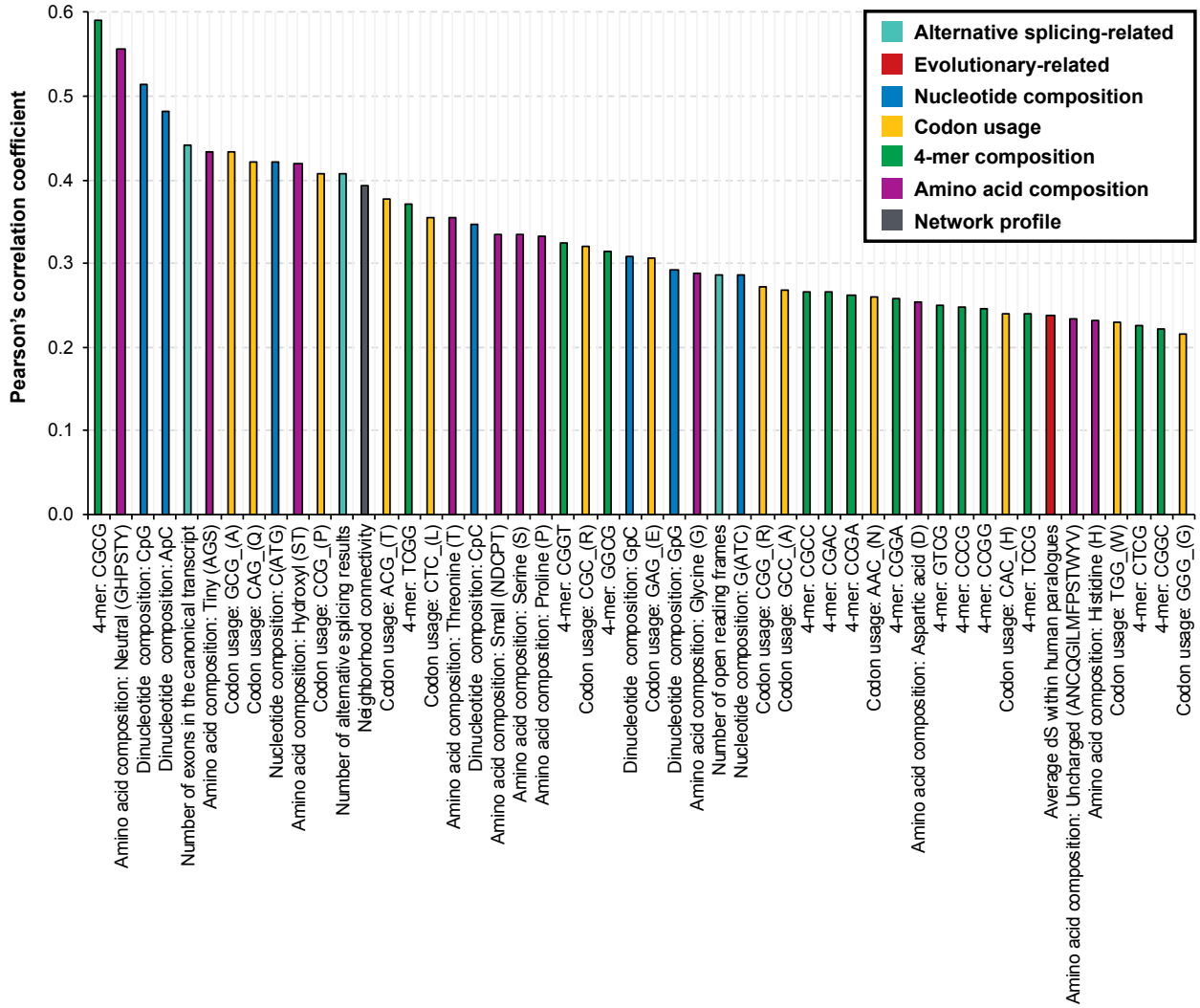

682

683 **Fig 11. 50 features negatively associated with higher up-regulation after IFN treatments in**
684 **human fibroblast cells (Student t-tests: $p < 0.05$).** Detailed results about PCC and hypothesis tests
685 are provided in **S3 Data**. Abbreviations: IFNs, interferons; PCC, Pearson's correlation coefficient; dS,
686 synonymous substitutions per synonymous site.

687

688 **Difference in feature representation of interferon-repressed genes and genes with low levels of**
689 **expression**

690 We group human genes into two classes based on their response to the type I IFNs in human fibroblast
691 cells. Genes significantly up-regulated in the IFN experiments are included in the ISG class, while
692 those that do not are put into the non-ISG class. However, there is also another group of genes down-
693 regulated in the presence of IFNs, i.e., IRGs. They are labelled as non-ISGs, but contain unique
694 patterns that constitute an important aspect of the IFN response [8]. Some of these IRGs are not up-
695 regulated in any known type I IFN systems, thus have been placed in a refined non-ISGs class for
696 analyses and predictions. Additionally, there are a number of genes that have insufficient levels of

expression in the experiments to determine a fold change. Here, we use the previously defined features to compare ISG with IRGs and ELGs.

As shown in **Fig 12,** IRGs are differentially represented to a lower extent in the majority of nucleotide 4-mer compositions than ISGs, which indicates the deficiency of some nucleotide sequence patterns in the coding region of IRGs. Note that, many nucleotide 4-mer composition features are more suppressed in ISGs than non-ISGs although the differences are small. The biased representation of these features in IRGs suggests that IRGs have characteristics similar to ISGs rather than non-ISGs. Additionally, there are a very limited number of features relating to evolutionary conservation, nucleotide compositions or codon usages showing obvious differences between ISGs and IRGs, but many of them are differentially represented when comparing ISGs with non-ISGs. Therefore, involving IRGs in the class of non-ISGs will increase the risk for machine learning models to produce more false positives. However, there are some informative features differentiating IRGs from ISGs. For example, comparing with ISGs, IRGs are more enriched in CpGs (Mann-Whitney U test: p = 5.6E-03), which is also mentioned in [70]. IRGs tend to have higher closeness centrality and neighbourhood connectivity than ISGs (Mann-Whitney U test: p = 0.04 and 6.4E-06 respectively), suggesting IRGs tend to be closer to the centre of the human PPI network and connected to key proteins with many interaction partners. Differences in some amino acid composition features between ISGs and IRGs can also be observed. Therefore, good predictability is still expected when using features extracted from proteins sequences.

Fig 12 illustrates 161 features showing significant differences (Mann-Whitney U tests: $p < 0.05$) in the representation of ISGs and ELGs. An estimated 82% of these features are also differentially represented between ISGs and non-ISGs. 79% of these significant features show similar over-representation or under-representation in two comparisons, i.e., ISGs versus ELGs and ISGs versus non-ISGs. These ratios indicate that the majority of ELGs are less likely to be ISGs based on their feature profile as well as their low expression levels in cells induced with IFNs. Network analyses show that ELG products tend to have lower values of all calculated network features with the exception of topological coefficient than ISG products, suggesting that they are less connected by other human proteins in the human PPI network. Particularly, their abnormal representation on the feature of average shortest paths indicating that some ELGs may still have high connectivity in the human PPI network, e.g., vascular cell adhesion molecule 1 (VCAM1) and ubiquitin D (UBD).

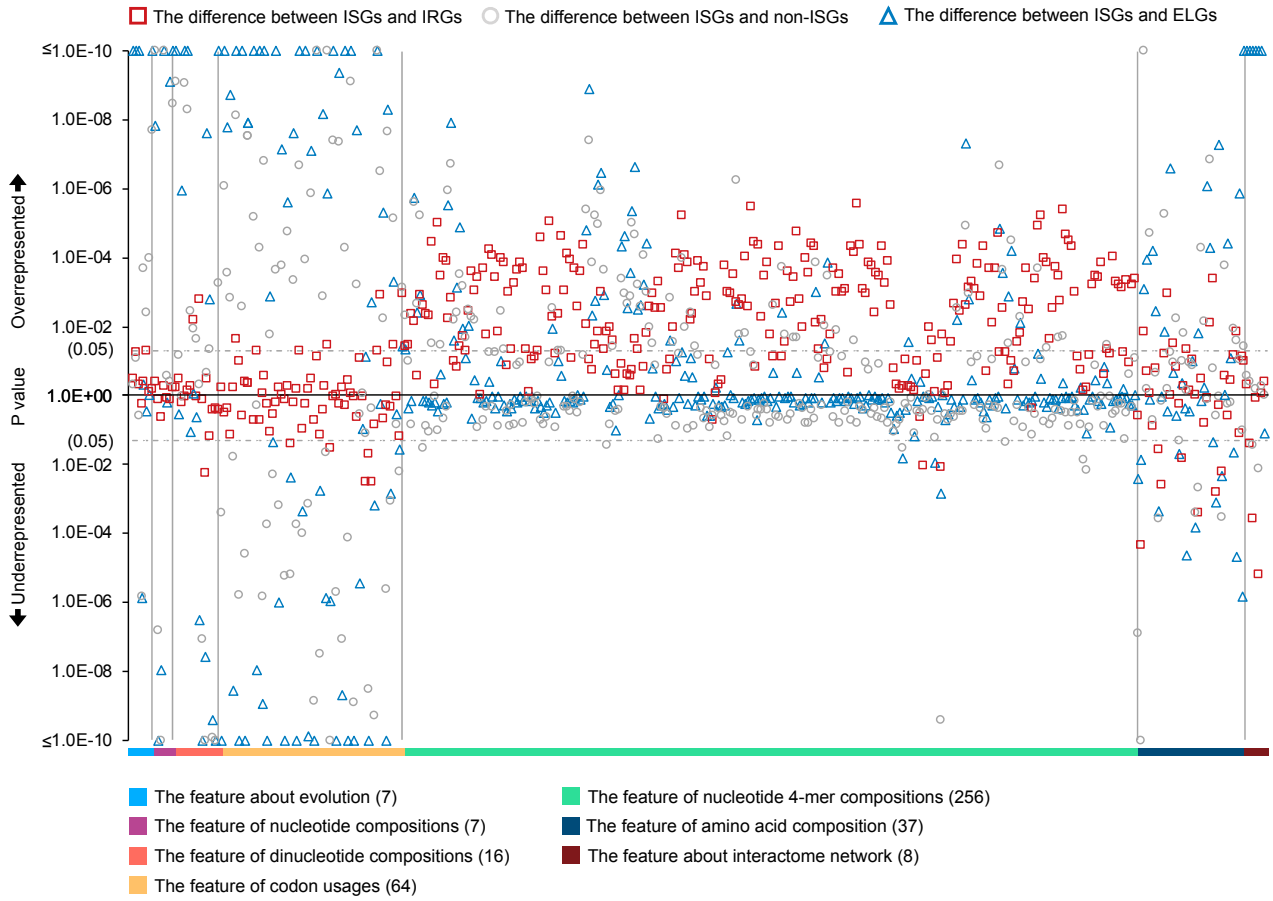

Fig 12. Differential expressions of parametric features between different genes and their coded proteins. Mann-Whitney U tests are applied for hypothesis testing and the results were provided in the **S2 Data**. Here, ISGs and non-ISGs are taken from dataset S2; IRGs and ELGs are taken from dataset S1; the background human genes are from dataset S1. Abbreviations: ISGs, interferon-upregulated genes; IRGs, interferon-repressed genes; non-ISGs, human genes not significantly up-regulated by interferons; ELGs, expression-limited human genes in IFN experiments.

Implementation with machine learning framework

In this study, we encode 397 parametric and 7046 non-parametric features for the analyses. As an excess of features will greatly increase the dimension of feature spaces and complicate the classification task for SVM [53], we limit the number of SLim_DNAs to the top 100 based on the adjusted p-value and we expect these to be sufficient to provide a picture of SLim patterns in the coding region of the canonical transcript. Accordingly, features measuring the co-occurrence status of multiple SLim_DNAs are recalculated based on the selected 100 SLim_DNAs. To reduce the impact of noisy data toward classifications, we only use the refined ISGs and non-ISGs, i.e., dataset S2 in machine learning.

Measured by SN, SP, MCC and AUC, the initial prediction results shown in **Table 4** indicate that proteome-based features, including those deciphered from protein sequences and the human interactome, perform much better than genome-based features presumably due to overfitting of the model [71]. Using parametric features that take advantage of both genetic and proteomic aspects shows a good improvement in tests. The non-parametric features used in this study give a binary statement for the occurrence of SLims in genetic and proteomic sequences but seem not to perform well and disrupt the model when they are combined with parametric features. The results shown in the previous analyses also indicate that there are a considerable number of disruptive features hidden in the set (**Fig. 5, Fig 7, and Fig 9**). The similar attributes of ISGs and IRGs (**Fig. 12**) lead to lots of noisy data biasing the classifiers. This situation is not ameliorated and becomes more difficult when using other machine learning algorithms such as k-nearest neighbors (KNN), decision tree (DT), random forest (RF) (**Table 4**) [72, 73]. As some genes respond to IFNs in a cell-specific manner [2], it is hard to produce predictions unless we detect key discriminating features, which are robust to the change of biological environment.

Considering these drawbacks, we design an AUC-driven subtractive iteration algorithm (ASI) (**Fig 2**) to remove as many disruptive features as possible (**Fig 13A**). Pre-processing using the ASI algorithm shows that there are at least 28% of bad features disrupting the prediction model. They include 34% of features on codon usages and 50% of SLim features, thus, explaining the poor performance of the model trained with non-parametric features (**Table 4**). However, the loss of some of the individual nucleotide 4-mer feature seems not to influence the performance of the classifier at this stage, but the similarities between IRGs and ISGs (**Fig 12**) particularly in these 4-mer features is a cause for concern when the model is used to predict new data especially unknown IRGs. When using the ASI algorithm, the number of disrupting features does not stabilise and until the algorithm reaches the 11-th iterations when the number of disrupting features becomes zero. The remaining 74 features constitute our optimum feature set for the prediction of ISGs (**Table 5**). Among them, 14 and 9 features have positive and negative correlations with the level of up-regulation in IFN experiments. During the procedure, the AUC keeps increasing and reaches 0.7479 after 11 iterations. The MCC also shows an overall improvement although it fluctuates slightly during the last few iterations. By degressively ranking the probability calculated by the prediction model, we found 68.1% of the 496 genes (equal to the number of ISGs in the training dataset) are successfully predicted as ISGs. **Fig 13B** illustrates the distribution of probability scores generated by the ASI-optimised model for human genes with different expressions in IFN experiments. Human genes with higher up-regulation in IFN experiments tend to obtain higher probability score from our optimised machine learning model (PCC = 0.243, p = 4.2E-10). However, there are also some ISGs incorrectly predicted by our model even though they are

highly up-regulated, e.g., basic leucine zipper ATF-like transcription factor 2 (BATF2, probability score = 0.34). The model produces 33 ISGs with a probability score higher than 0.8 but such figure for non-ISGs reduces to six, including one IRG, i.e., tripartite motif containing 59 (TRIM59). The highest probability score within non-ISGs was found on ubiquitin conjugating enzyme E2 R2 (UBE2R2, probability score = 0.88). It contains many features similar to ISGs but is not differentially expressed in the presence of IFN in fibroblast cells [8]. The lowest probability score within ISGs is found on cap methyltransferase 1 (CMTR1, probability score = 0.12) due to the weak signal from its features. For example, CMTR1 protein does not contain any ISG-favoured SLim_AA listed in **Table 2**. The influence of IRGs on the prediction is reflected in the training dataset but is not significant. Compared with human genes not differentially expressed in the IFN experiments, i.e., non-ISGs but not IRGs, there are slightly more IRGs unsuccessfully classified when using a threshold of 0.549 (Pearson's chi-squared tests: $M_1 = 27\%$, $M_2 = 24\%$, $p > 0.05$).

Table 4. The performance of different feature combinations on the training dataset S2' via five-fold cross validation.

Method	Features	Number	Threshold-dependent					Threshold-independent	
			Score range	Threshold[a]	SN	SP	MCC	SN_496[b]	AUC
SVM	Genetic	452	0.359~0.623	0.402	0.769	0.355	0.169	0.579	0.6058
SVM	Proteomic	66	0.261~0.730	0.560	0.425	0.778	0.218	0.605	0.6360
SVM	Parametric	397	0.305~0.760	0.529	0.595	0.665	0.261	0.621	0.6573
SVM	Non-parametric	121	0.368~0.605	0.487	0.653	0.504	0.159	0.573	0.5736
SVM	All	518	0.328~0.743	0.542	0.567	0.681	0.250	0.615	0.6509
KNN[c]	All	518	0.100~0.900	0.500~0.550	0.593	0.621	0.214	0.607±0.014	0.6305
DT	Partial	182[d]	0 or 1	N/A	0.546	0.548	0.095	0.546	N/A
RF[e]	Random	Random	0.080~0.900	0.380~0.579	0.590±0.168	0.617±0.183	0.219±0.019	0.600±0.007	0.6413±0.0082
SVM	Optimum	74	0.098~0.918	0.549	0.623	0.750	0.376	0.681	0.7479

*[a]this threshold is provided by maximum the value of MCC; [b]this sensitivity is measured among tested genes with the top 496 prediction probabilities; [c]k-value here is set as the square root of the size of the training samples in five-fold cross validation, i.e., k = 20 [74]; [d]182 out of the 518 features (**S5 Data**) are used for decisions during this modelling procedure as the rest ones are not helpful to better split the dataset for lower system entropy [75]; [e]this random forest algorithm uses 50 random grown trees and the modelling and validation procedures are repeated for 10 times.*

Abbreviations: SVM, support vector machine; KNN, k-nearest neighbors; DT, decision tree; RF, random forest; SN, sensitivity; SP, specificity; MCC, Matthews correlation coefficient; AUC, area under the receiver operating characteristic curve.

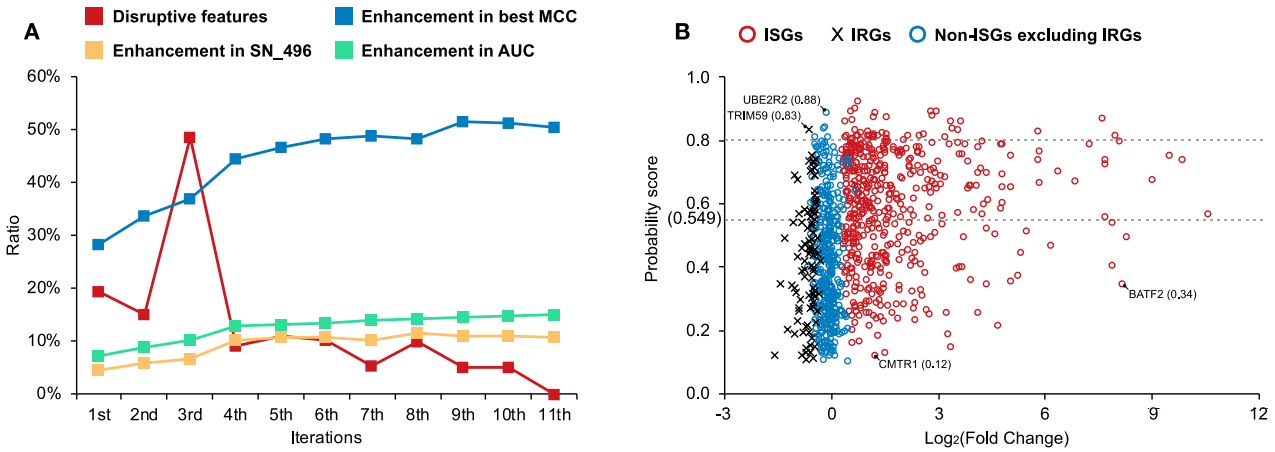

Fig 13. The optimisation on the machine learning model with the ASI algorithm. (A) shows the change of the prediction models based on the one generated with all 518 features (disruptive feature vector = 144, best MCC = 0.250, SN_496 = 0.615, and AUC = 0.6509). (B) shows the distribution of probability scores generated by the ASI-optimised model for human genes with different expression levels in the IFN system. ISGs and non-ISGs shown in (B) are randomly selected with an undersampling strategy on dataset S2. The list of gene names can be found in **S1 Data**. Abbreviations: SN, sensitivity; SN_496, sensitivity of predicted genes with the top 496 probability scores, MCC, Matthews correlation coefficient; AUC, area under the receiver operating characteristic curve; ASI, AUC-driven subtractive iteration algorithm; IFN, interferon, ISGs, interferons-stimulated genes; IRGs, interferon-repressed genes; non-ISGs, interferons-non-up-regulated genes; UBE2R2, ubiquitin conjugating enzyme E2 R2; TRIM59, tripartite motif containing 59; CMTR1, cap methyltransferase 1; BATF2, basic leucine zipper ATF-like transcription factor 2.

Table 5. The optimum 74 features contributing to the prediction of ISGs.

Evolutionary features (2)		
Number of human paralogues^{P}, average dS within human paralogues^{P-}.		
Codon usage features (10)		
Codon usage: CTA (L)$^{P+}$	Codon usage: ATT (I)^{P}	Codon usage: TAT (Y)^{P}
Codon usage: GCG (A)$^{P-}$	Codon usage: CAC (H)$^{P-}$	Codon usage: TGC (C)^{P}
Codon usage: CGT (R)^{P}	Codon usage: CGA (R)^{P}	Codon usage: CGG (R)$^{P-}$
Codon usage: AGA (R)$^{P+}$		
Genetic composition features (40)		
DNA AC content^{P}	Dinucleotide CpT composition^{P}	DNA 4-mer CGCG composition^{P-}
DNA 4-mer AATC composition^{P+}	DNA 4-mer TCGT composition^{P}	DNA 4-mer GATG composition^{P+}
DNA 4-mer AACA composition^{P}	DNA 4-mer TGAG composition^{P+}	DNA 4-mer GACC composition^{P}
DNA 4-mer ATAT composition^{P}	DNA 4-mer TGTA composition^{P}	DNA 4-mer GACG composition^{P}

DNA 4-mer ATGT composition^{P+}	DNA 4-mer CACG composition^{P}	DNA 4-mer GAGT composition^{P+}
DNA 4-mer ACAC composition^{P}	DNA 4-mer CTCC composition^{P}	DNA 4-mer GTAC composition^{P}
DNA 4-mer ACTA composition^{P}	DNA 4-mer CCAC composition^{P}	DNA 4-mer GTGT composition^{P}
DNA 4-mer ACTC composition^{P}	DNA 4-mer CCTA composition^{P}	DNA 4-mer GTGC composition^{P}
DNA 4-mer ACCG composition^{P}	DNA 4-mer CCTC composition^{P+}	DNA 4-mer GTGG composition^{P}
DNA 4-mer TATG composition^{P}	DNA 4-mer CCGT composition^{P}	DNA 4-mer GCAA composition^{P+}
DNA 4-mer TTCT composition^{P}	DNA 4-mer CGAG composition^{P}	DNA 4-mer GCTC composition^{P}
DNA 4-mer TTCG composition^{P}	DNA 4-mer CGTG composition^{P}	DNA 4-mer GCCT composition^{P}
DNA 4-mer TTGA composition^{P}	DNA 4-mer CGCA composition^{P}	DNA 4-mer GGGG composition^{P}
DNA 4-mer TCAT composition^{P}		
Proteomic composition features (9)		
Arginine composition^{P}, cysteine composition^{P+}, methionine composition^{P};		
Basic amino acid composition (R/H/K)$^{P+}$		Sulfur amino acid composition (C&M)$^{P+}$
Hydroxyl amino acid composition (S&T)$^{P-}$		Small amino acid composition (N/D/C/P/T)$^{P-}$
Large amino acid composition (R/I/L/K/M)$^{P+}$		
Uncharged amino acid composition (A/N/C/Q/G/I/L/M/F/P/S/T/W/Y/V)$^{P-}$		
Features about human interactome network (3)		
Shortest paths^{P+}, betweenness^{P}, neighborhood connectivity^{P-}.		
Motif features (8)		
SLim_DNA ATA[AG][TG]^{N}	SLim_DNA TAT[AT]T^{N}	SLim_DNA T[AT]AAA^{N}
SLim_DNA [ATG]TGTA^{N}	SLim_AA S[A-Z]N[A-Z]E^{N}	SLim_AA ENE^{N}
SLim_AA SVI^{N}	Co-occurence of SLim_AAs^{P}	

^{P}parametric features; ^{N}non-parametric features; $^{+}$means features are positively associated with the level of up-regulation in IFN experiments ($p < 0.05$); $^{-}$means features are negatively associated with the level of up-regulation in IFN experiments ($p < 0.05$).

Abbreviations: dS, synonymous substitutions per synonymous site; SLim_DNAs, short linear nucleotide motifs; SLim_AAs, short linear amino acid motifs.

Review of different testing datasets

In this study, we train and optimise a SVM model from our training dataset, i.e., S2', and prepare seven testing datasets to assess the generalisation capability of our model under different conditions. The S2'' testing dataset is a subset of dataset S2. The prediction performance on this testing dataset is close to that in the training stage with an AUC of 0.7455 (**Fig. 14**). The best MCC value is achieved when setting the judgement threshold to 0.438, which means that the prediction model is sensitive to signals related to ISGs. In this case, it produces predictions with high sensitivity but inevitably produces many false positives, especially within the IRG class.

In the S3 testing dataset, we use 695 ISGs with low confidence. The overall accuracy only reaches 44.0% when using a judgement threshold of 0.549, about 18% lower than SN under the same threshold in the training dataset S2' (**Table 4**). This is expected as they have some inherent attributes

that make them slightly up-regulated, silent or even repressed (e.g., become non-ISGs in other IFN systems) in response to some IFN-triggered signalling. On the other hand, on the S3 testing dataset, our machine learning model produces 38 (5.5%) ISGs with a probability score higher than 0.8. This number is also lower than on the training dataset S2', which further indicates the relatively low confidence for ISGs included in testing dataset S3.

The S4 testing dataset is constructed to illustrate our hypothesis that there are some patterns shared among ISGs and IRGs at least in the type I IFN system in human fibroblast cells. On this testing dataset, the prediction accuracy is 60.2% under the judgement threshold of 0.549, about 15% lower than the SP under the same threshold in the training dataset S2' (**Table 4**). Leucine rich repeat containing 2 (LRRC2), carbohydrate sulfotransferase 10 (CHST10) and eukaryotic translation elongation factor 1 epsilon 1 (EEF1E1) show strong signals of being ISGs (probability score > 0.9). In total, there are 56 (5.6%) IRGs being incorrectly predicted as ISGs with probability scores higher than 0.8. This high score is found in an estimated 8.1% of ISGs but is only observed in 1.2% of human genes not differentially expressed in the IFN experiments (**Fig 13B**). This result indicates that there is a considerable number of IRGs incorrectly predicted as ISGs in S4 testing dataset due to close distance to the ISGs in the high-dimensional feature space and this may be the case for any of the datasets. It also supports our hypothesis about the shared patterns from the machine learning aspect and is consistent with the results shown in **Fig 12**.

The next three testing datasets, i.e., S5, S6, and S7 are collected from the Interferome database [21] to test the applicability of the machine learning model across different IFN types. The ISGs in these testing datasets are all highly up-regulated (Log_2(Fold Change) > 1.0) in the corresponding IFN systems while all the non-ISGs are not up-regulated after corresponding IFN treatments (Log_2(Fold Change) < 0). The results shown in **Fig 14** reveals that ISGs triggered by type I or III IFN signalling can still be predicted by our machine learning model, but the performance is limited (AUC = 0.6677 and 0.6754 respectively). However, it is almost impossible to make normal predictions with the current feature space for human genes up-regulated by type II IFNs (AUC = 0.5532).

The S8 testing dataset consists of 2217 human genes that are insufficiently expressed in the experiments in human fibroblast cells [8]. The results show that there are around 41.2% ELGs being predicted as ISGs when using a judgement threshold of 0.549. This is approximately 21% lower than the SN under the same threshold in the training dataset S2' (**Table 4**). This suggests that there are more non-ISGs than ISGs in this dataset, which is consistent with the results of **Fig 12**. We find 10 ELGs with probability scores higher than 0.900: CD48 molecule, CD53 molecule, lipocalin 2 (LCN2), uncoupling protein 1 (UCP1), coiled-coil domain containing 68 (CCDC68), potassium calcium-activated channel subfamily M regulatory beta subunit 2 (KCNMB2), potassium voltage-gated channel

interacting protein 4 (KCNIP4), zinc finger HIT-type containing 3 (ZNHIT3), serpin family B member 4 (SERPINB4), and fibrinogen silencer binding protein (FSBP). By retrieving data from the Genotype-Tissue Expression project [76], we find the expression of these ELGs are generally limited with the exception of CD53 and ZNHIT3 (**Fig 15**). The expression data of CD53 is not included in the OCISG database [8] and are also limited in the Interferome database [21]. It only shows slight up-regulation after type I treatments in blood, liver, and brain but there is currently no record of its expression level in the presence of type I IFNs in human fibroblast cells. ZNHIT3 is another well-expressed gene lacking information in the OCISG. In the Interferome databases, we find that ZNHIT3 can be up-regulated after IFN treatments in some fibroblast cells on skin. As for the remaining eight ELGs, despite their limited expression in human fibroblast cells, their features suggest that they are very likely to be IFN-stimulated in a currently untested cell type.

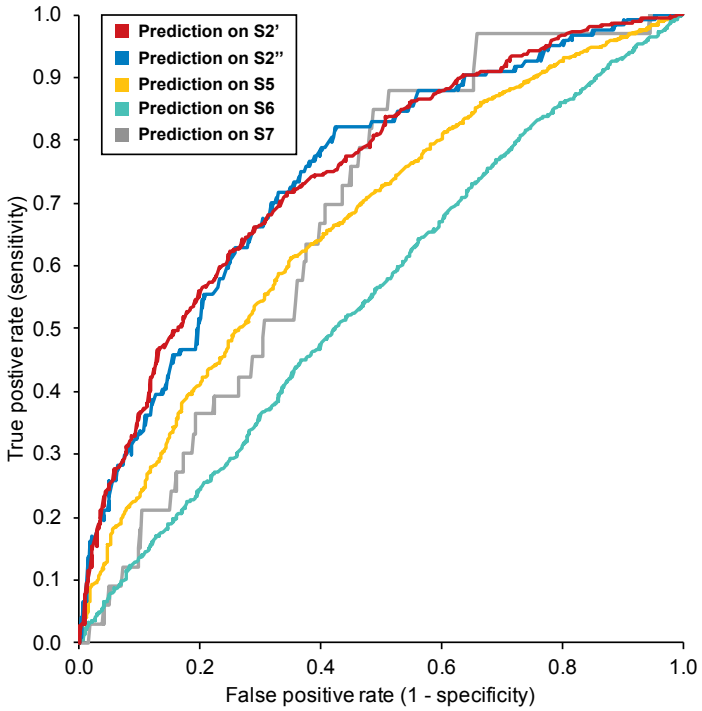

Fig 14. The performance of our optimised model on different datasets. S2' is the training dataset used in this study. It randomly includes 496 ISGs and an equal number of non-ISGs from dataset S2 that contains ISGs/non-ISGs with high confidence (**Table 1**). Evaluation on this dataset in (A) is processed via five-fold cross validation. S2'' is the testing dataset constructed with the remaining human genes in dataset S2. S5, S6, and S7 are collected from the Interferome database [21], including human genes with different responses to the type I, II and III IFNs, respectively. The label and usage of these human genes are provided in **S1 Data**. Abbreviations: AUC, area under the receiver operating

887 characteristic curve; ISGs, interferon-stimulated genes; non-ISGs, human genes not significantly up-
888 regulated by interferons.
889

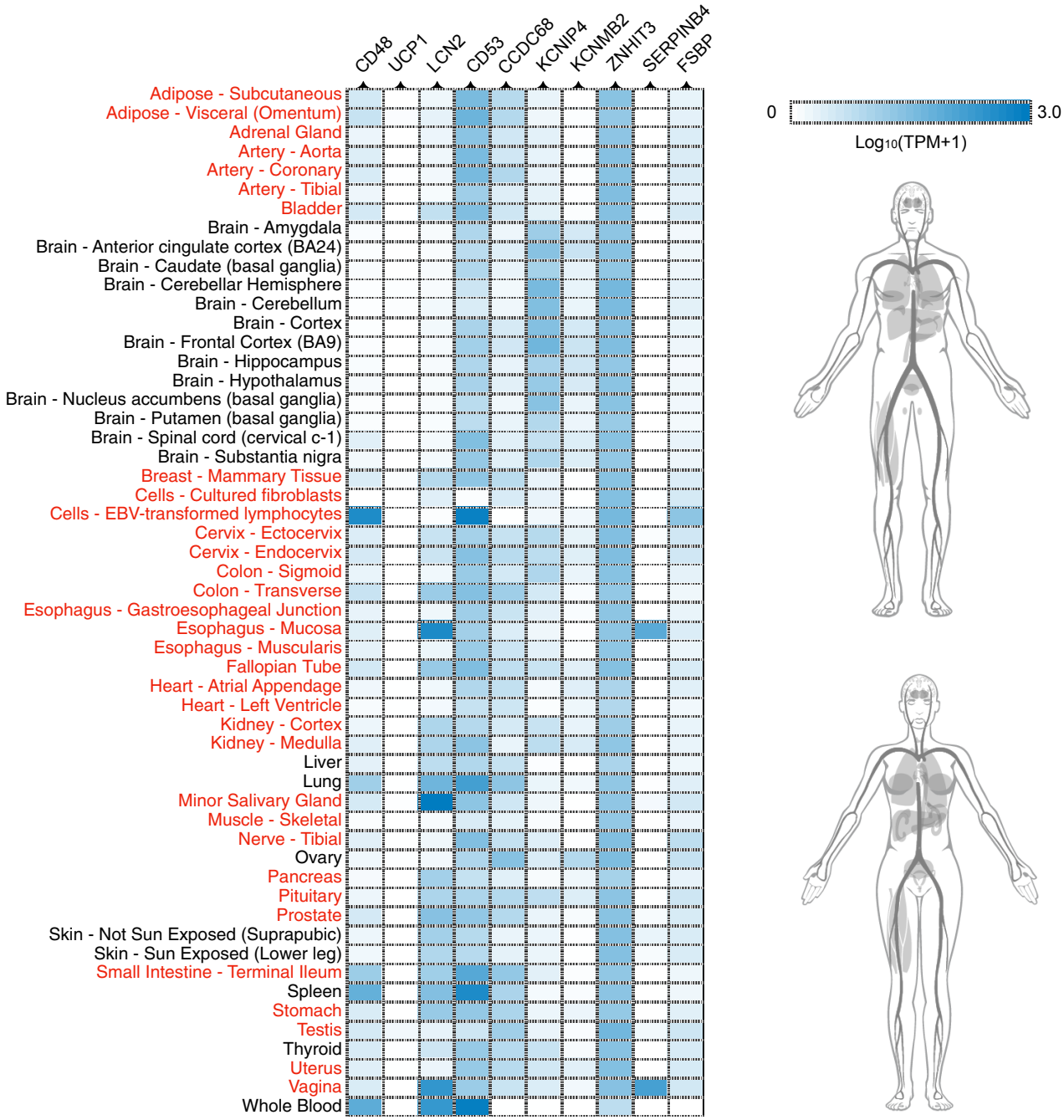

890

891 **Fig 15. Expression of ELGs in different tissues.** Expression data for ten ELGs are collected from
892 the Genotype-Tissue Expression project (https://gtexportal.org/) [76]. The tissues in red are not
893 included in the Interferome database [21]. White boxes in the heatmap indicate that there is no data
894 available for genes in the corresponding tissues. The overall expression level of these ten ELGs are
895 reflected via human perspective photo retrieved from Expression Atlas (https://www.ebi.ac.uk/gxa)
896 [77]. Abbreviations: ELGs, human genes with limited expression in interferon experiments; TPM,

transcripts per million; BA, Brodmann area; EBV, Epstein-Barr virus; UCP1, uncoupling protein 1; LCN2, lipocalin 2; CCDC68, coiled-coil domain containing 68; KCNIP4, potassium voltage-gated channel interacting protein 4; KCNMB2, potassium calcium-activated channel subfamily M regulatory beta subunit 2; ZNHIT3, zinc finger HIT-type containing 3; SERPINB4, serpin family B member 4; FSBP, fibrinogen silencer binding protein.

Discussion

In this study, we investigate the characteristics that influence the expression of human genes in type I IFN experiments. We compare ISGs and non-ISGs through multiple procedures to guarantee strong signals for ISGs and to avoid cell-specific influences that result in the lack of ISGs expression in certain cell types [2]. Even some highly up-regulated ISGs can become down-regulated when the biological conditions change, exemplified by the performance of C-X-C motif chemokine ligand 10 (CXCL10) on liver biopsies after IFN-α treatment. This refinement is necessary as the representation of features between ISGs and the background human genes show that many non-ISGs especially IRGs have similar feature patterns to ISGs (**Fig 4-7**, **Fig 12**).

Generally, ISGs are less evolutionarily conserved with more human paralogues than non-ISGs. They have specific nucleotide patterns exemplified by the depletion of GC-content and have a unique codon usage preference in coding proteins. There are a number of SLim_DNAs widely observed in the cDNA of ISGs which are relatively rare in non-ISGs (**S4 Data**). Likewise, there are also many SLim_AAs highlighted in the sequences of ISG products that are absent or rare in non-ISGs (**Table 2**). In the human PPI network, ISG products tend to have higher betweenness than background human protein, indicating their more frequent interruption of the shortest path (geodesic distance) between different nodes. Abnormal expression or knockout of these proteins will increase the diameter of the network and may lead to some lethal consequences that are not tolerated in signalling pathways [78-80]. These ISG specific patterns may be the result of the evolution of the innate immune system in vertebrates and could be adaptations to the cellular environment induced by interferon following a pathogenic infection [81]. It is also possible that some of the particular SLim_DNAs and SLim_AAs may be important functionally as the cell changes from non-infected to infected. Experimental evidence will be necessary to investigate this.

Some inherent properties of ISGs facilitate or elevate their expression after IFN treatments but may also be used by viruses to escape from IFN-mediated antiviral response [19]. For instance, the representation of dN shows a more significant difference than that of dS within human paralogues

Higher dN/dS ratio positively correlated with gene up-regulation following IFN treatments, but this means the gene is less conserved with more non-synonymous or nonsense mutations, which can often be associated to inherited diseases and cancer [82]. It will also facilitate the virus to interfere with IFN signalling through the JAK-STAT pathway and inactivate downstream cellular factors involved in IFN signal transductions [19]. Arginine is under-represented in ISG products compared to non-ISG products As arginine is essential for the normal proliferation and maturation of human T cells [83], such depletion in ISG products may leave a risk of inhibiting T-cell function and potentially increased susceptibility to infections [84]. On the other hand, the special pattern of ISGs also promotes the representation of some features even if they are not well represented in nature, exemplified by the higher cysteine composition in ISGs. We hypothesize that it may be helpful to activate T-cell to regulate protein synthesis, proliferation and secretion of immunoregulatory cytokines [85, 86]. For example, there are also some features, e.g., methionine composition, not differentially represented between ISGs and non-ISGs that play important roles in IFN-mediated immune responses. There is evidence for the methionine content playing a role in the biosynthesis of S-Adenosylmethionine (SAM), which can improve interferon signalling in cell culture [87, 88].

As previously mentioned, there are similar patterns between the feature representation of ISGs and IRGs, which leads to the unclear boundary for ISGs and non-ISGs in the feature space. We find significant differences on the representation of features on evolutionary conservation (**Fig 4**) between ISGs and non-ISGs, but these become non-significant when comparing ISGs with IRGs. Similar phenomena are observed on many features deciphered from the canonical transcript, e.g., dinucleotide composition and codon usage features. We suggest that IRGs can be viewed as additional ISGs as they also regulate the activity of human genes in response to IFNs, only negatively. On the other hand, despite so many similarities between ISGs and IRGs, the separate classification of these genes is still possible. 4-mer compositions can be considered as the key features as most of them are differentially represented between ISGs and IRGs (**Fig 12**). Using proteomic features can also help to differentiate ISGs from IRGs but is not as good as using 4-mer features.

In the machine learning framework, we develop the ASI algorithm to remove disruptive features but keep features not influencing the prediction performance when being removed individually during iterations. Features may have synergistic effects thus the elimination of each feature leaves a different impact on the remaining ones even if these are individually useless for the improvement of the classifier. In this case, keeping as many useful features as possible seems to be a good option but will greatly increase the dimension of the feature space and the risk of overfitting [71]. By contrast, our ASI algorithm avoids such a risk and keeps the synergistic effect of different features through iterations.

In the prediction task, we find some previously labelled non-ISGs with very high probability scores, suggesting that they have many inherent properties enabling them to be stimulated after IFN treatments. Some of them, for example UBE2R2 has been shown to be significantly up-regulated after IFN-α treatment [89]. The non-ISG label was assigned because the relevant expression data in the presence of IFNs are not included in the OCISG [8] and the Interferome databases [21]. We also find ten ELGs with very high probability scores (> 0.9). Literature searches on these genes indicate that they are likely to be involved in the innate immune response and that their responses may be limited to certain tissues or cell types for which there is limited expression data in the Interferome database [21]. For example, LCN2 has been shown to mediate an innate immune response to bacterial infections by sequestering iron [90] and is induced in the central nervous system of mice infected with West Nile virus encephalitis [91]. CD48 was shown to increase in levels as a result of human IFN-α/β and human IFN-γ and these upregulate the expression of CD48 proteins at the surface of various cultured human cell lines [92]. Interestingly, CD48 is also the target of immune evasion by viruses [93] and has been captured in the genome of cytomegalovirus and undergone duplication [94]. Evidence for other ELGs is harder to assess, particularly those for which expression is absent in a range of tissues (e.g., UCP1 in **Fig 15**). UCP1 is a mitochondrial carrier protein expressed in brown adipose tissue (BAT) responsible for non-shivering thermogenesis [95]. It is possible that UCP1 is stimulated directly or indirectly by IFN in BAT resulting in the defended elevation of body temperature in response to infection. In this in silico study, we provide predictions for genes that show no basal expression in human fibroblasts but their stimulation by IFN and their role in immune defense requires testing experimentally.

The model developed in this study based on experimental data from human fibroblast cells stimulated by IFN can be generalised to type III systems, presumably because activations of type I and III ISGs are both controlled by ISRE [9] and aim to regulate host immune response [4-6]. However, our model cannot be applied to the prediction of type II ISGs (AUC = 0.5532), not only because of their different control elements, but because of their different roles in human immune activities (**Fig 1**) [10].

In summary, our analyses highlight some key sequence-based features that are helpful to distinguish ISGs from non-ISGs or IRGs. Our machine learning model is able to produce a list of putative ISGs to support IFN-related research. As knowledge of ISG functions continue to be elucidated by experimentalists, the *in-silico* approach applied here could in future be extended to classify the different functions of ISGs.

Supporting information

S1 Data. Basic information about human genes used in this study.
(TXT)

S2 Data. The result of Mann-Whitney U tests for parametric features.
(TXT)

S3 Data. Association between feature representations and IFN stimulations.
(TXT)

S4 Data. The result of Pearson's chi-squared tests for sequence motifs.
(TXT)

S5 Data. Decision trees generated during five-cross validation on the training dataset S2'.
(TXT)

Acknowledgments

The authors wish to thank Prof Andrew Davison, Drs Suzannah Rihn and Sam Wilson for helpful discussions and recommendations, and Scott Arkison for help setting up the website.

Author contributions

Conceptualization: David L. Robertson, Joseph Hughes, Quan Gu, Haiting Chai.

Data curation: Haiting Chai.

Formal analysis: Haiting Chai.

Funding acquisition: Haiting Chai, David L. Robertson.

Webserver: Haiting Chai.

Supervision: David L. Robertson, Joseph Hughes, Quan Gu.

Writing-original draft: Haiting Chai.

Writing-review & editing: David L. Robertson, Joseph Hughes, Quan Gu, Haiting Chai.

Data availability statement

The implemented web server and data were freely accessible at http://isgpre.cvr.gla.ac.uk/.

Funding

HC: China Scholarship Council under Grant 201706620069. JH, QG and DLR: Medical Research Council (MC_UU_1201412). The funders had no role in study design, data collection and analysis, decision to publish, or preparation of the manuscript.

Competing interests

The authors have declared that no competing interests exist.

References

1. Rönnblom L. The type I interferon system in the etiopathogenesis of autoimmune diseases. Ups J Med Sci. 2011; 116(4): 227-237. https://doi.org/10.3109/03009734.2011.624649 PMID: 22066971
2. Mostafavi S, Yoshida H, Moodley D, LeBoité H, Rothamel K, Raj T, et al. Parsing the interferon transcriptional network and its disease associations. Cell. 2016; 164(3): 564-578. https://doi.org/10.1016/j.cell.2015.12.032 PMID: 26824662
3. De Weerd NA, Samarajiwa SA, Hertzog PJ. Type I interferon receptors: biochemistry and biological functions. J Biol Chem. 2007; 282(28): 20053-20057. https://doi.org/10.1074/jbc.R700006200 PMID: 17502368
4. Kotenko SV, Durbin JE. Contribution of type III interferons to antiviral immunity: location, location, location. J Biol Chem. 2017; 292(18): 7295-7303. https://doi.org/10.1074/jbc.R117.777102 PMID: 28289095
5. Fensterl V, Sen GC. Interferons and viral infections. Biofactors. 2009; 35(1): 14-20. https://doi.org/10.1002/biof.6 PMID: 19319841
6. Lazear HM, Schoggins JW, Diamond MS. Shared and distinct functions of type I and type III interferons. Immunity. 2019; 50(4): 907-923. https://doi.org/10.1016/j.immuni.2019.03.025 PMID: 30995506
7. Takaoka A, Yanai H. Interferon signalling network in innate defence. Cell Microbiol. 2006; 8(6): 907-922. https://doi.org/10.1111/j.1462-5822.2006.00716.x PMID: 16681834
8. Shaw AE, Hughes J, Gu Q, Behdenna A, Singer JB, Dennis T, et al. Fundamental properties of the mammalian innate immune system revealed by multispecies comparison of type I interferon responses. PLoS Biol. 2017; 15(12): e2004086. https://doi.org/10.1371/journal.pbio.2004086 PMID: 29253856

9. Schneider WM, Chevillotte MD, Rice CM. Interferon-stimulated genes: a complex web of host defenses. Annu Rev Immunol. 2014; 32: 513-545. https://doi.org/10.1146/annurev-immunol-032713-120231 PMID: 24555472

10. Stark GR, Darnell Jr JE. The JAK-STAT pathway at twenty. Immunity. 2012; 36(4): 503-514. https://doi.org/10.1016/j.immuni.2012.03.013 PMID: 22520844

11. Schoggins JW. Interferon-stimulated genes: what do they all do? Annu Rev Virol. 2019; 6: 567-584. https://doi.org/10.1146/annurev-virology-092818-015756 PMID: 31283436

12. Aso H, Ito J, Koyanagi Y, Sato K. Comparative description of the expression profile of interferon-stimulated genes in multiple cell lineages targeted by HIV-1 infection. Front Microbiol. 2019; 10: 429. https://doi.org/10.3389/fmicb.2019.00429 PMID: 30915053

13. Dang W, Xu L, Yin Y, Chen S, Wang W, Hakim MS, et al. IRF-1, RIG-I and MDA5 display potent antiviral activities against norovirus coordinately induced by different types of interferons. Antiviral Res. 2018; 155: 48-59. https://doi.org/10.1016/j.antiviral.2018.05.004 PMID: 29753657

14. Masola V, Bellin G, Gambaro G, Onisto M. Heparanase: A multitasking protein involved in extracellular matrix (ECM) remodeling and intracellular events. Cells. 2018; 7(12): 236. https://doi.org/10.3390/cells7120236 PMID: 30487472

15. Schoggins JW. Recent advances in antiviral interferon-stimulated gene biology. F1000Research. 2018; 7. https://doi.org/10.12688/f1000research.12450.1 PMID: 29568506

16. Spence JS, He R, Hoffmann H-H, Das T, Thinon E, Rice CM, et al. IFITM3 directly engages and shuttles incoming virus particles to lysosomes. Nat Chem Biol. 2019; 15(3): 259-268. https://doi.org/10.1038/s41589-018-0213-2 PMID: 30643282

17. Haller O, Staeheli P, Schwemmle M, Kochs G. Mx GTPases: dynamin-like antiviral machines of innate immunity. Trends Microbiol. 2015; 23(3): 154-163. https://doi.org/10.1016/j.tim.2014.12.003 PMID: 25572883

18. Ivashkiv LB, Donlin LT. Regulation of type I interferon responses. Nat Rev Immunol. 2014; 14(1): 36-49. https://doi.org/10.1038/nri3581 PMID: 24362405

19. García-Sastre A. Ten strategies of interferon evasion by viruses. Cell Host Microbe. 2017; 22(2): 176-184. https://doi.org/10.1016/j.chom.2017.07.012 PMID: 28799903

20. Giotis ES, Robey RC, Skinner NG, Tomlinson CD, Goodbourn S, Skinner MA. Chicken interferome: avian interferon-stimulated genes identified by microarray and RNA-seq of primary chick embryo fibroblasts treated with a chicken type I interferon (IFN-α). Vet Res. 2016; 47(1): 1-12. https://doi.org/10.1186/s13567-016-0363-8 PMID: 27494935

21. Rusinova I, Forster S, Yu S, Kannan A, Masse M, Cumming H, et al. Interferome v2. 0: an updated database of annotated interferon-regulated genes. Nucleic Acids Res. 2012; 41(D1): D1040-D1046. https://doi.org/10.1093/nar/gks1215 PMID: 23203888

22. OhAinle M, Helms L, Vermeire J, Roesch F, Humes D, Basom R, et al. A virus-packageable CRISPR screen identifies host factors mediating interferon inhibition of HIV. Elife. 2018; 7: e39823. https://doi.org/10.7554/eLife.39823 PMID: 30520725

23. Zhang Y, Burke CW, Ryman KD, Klimstra WB. Identification and characterization of interferon-induced proteins that inhibit alphavirus replication. J Virol. 2007; 81(20): 11246-11255. https://doi.org/10.1128/JVI.01282-07 PMID: 17686841

24. Pamela C, Kanchwala M, Liang H, Kumar A, Wang L-F, Xing C, et al. The IFN response in bats displays distinctive IFN-stimulated gene expression kinetics with atypical RNASEL induction. The Journal of Immunology. 2018; 200(1): 209-217. https://doi.org/10.4049/jimmunol.1701214 PMID: 29180486

25. Feld JJ, Nanda S, Huang Y, Chen W, Cam M, Pusek SN, et al. Hepatic gene expression during treatment with peginterferon and ribavirin: Identifying molecular pathways for treatment response. Hepatology. 2007; 46(5): 1548-1563. https://doi.org/10.1002/hep.21853 PMID: 17929300

26. Trilling M, Bellora N, Rutkowski AJ, de Graaf M, Dickinson P, Robertson K, et al. Deciphering the modulation of gene expression by type I and II interferons combining 4sU-tagging, translational arrest and in silico promoter analysis. Nucleic Acids Res. 2013; 41(17): 8107-8125. https://doi.org/10.1093/nar/gkt589 PMID: 23832230

27. O'Leary NA, Wright MW, Brister JR, Ciufo S, Haddad D, McVeigh R, et al. Reference sequence (RefSeq) database at NCBI: current status, taxonomic expansion, and functional annotation. Nucleic Acids Res. 2016; 44(D1): D733-D745. https://doi.org/10.1093/nar/gkv1189 PMID: 26553804

28. Yu X, Liu H, Hamel KA, Morvan MG, Yu S, Leff J, et al. Dorsal root ganglion macrophages contribute to both the initiation and persistence of neuropathic pain. Nat Commun. 2020; 11(1): 1-12. https://doi.org/10.1038/s41467-019-13839-2 PMID: 31937758

29. Chen Y, Lun AT, Smyth GK. From reads to genes to pathways: differential expression analysis of RNA-Seq experiments using Rsubread and the edgeR quasi-likelihood pipeline. F1000Research. 2016; 5. https://doi.org/10.12688/f1000research.8987.2 PMID: 27508061

30. Herrero J, Muffato M, Beal K, Fitzgerald S, Gordon L, Pignatelli M, et al. Ensembl comparative genomics resources. Database. 2016; 2016: bav096. https://doi.org/10.1093/database/bav096 PMID: 26896847

31. Yates AD, Achuthan P, Akanni W, Allen J, Allen J, Alvarez-Jarreta J, et al. Ensembl 2020. Nucleic Acids Res. 2020; 48(D1): D682-D688. https://doi.org/10.1093/nar/gkz966 PMID: 31691826

32. Li HD, Menon R, Omenn GS, Guan Y. Revisiting the identification of canonical splice isoforms through integration of functional genomics and proteomics evidence. Proteomics. 2014; 14(23-24): 2709-2718. https://doi.org/10.1002/pmic.201400170 PMID: 25265570

33. Sieber P, Platzer M, Schuster S. The definition of open reading frame revisited. Trends Genet. 2018; 34(3): 167-170. https://doi.org/10.1016/j.tig.2017.12.009 PMID: 29366605

34. Wang ET, Sandberg R, Luo S, Khrebtukova I, Zhang L, Mayr C, et al. Alternative isoform regulation in human tissue transcriptomes. Nature. 2008; 456(7221): 470-476. https://doi.org/10.1038/nature07509 PMID: 18978772

35. Bragg JG, Potter S, Bi K, Moritz C. Exon capture phylogenomics: efficacy across scales of divergence. Mol Ecol Resour. 2016; 16(5): 1059-1068. https://doi.org/10.1111/1755-0998.12449 PMID: 26215687

36. Pan Q, Shai O, Lee LJ, Frey BJ, Blencowe BJ. Deep surveying of alternative splicing complexity in the human transcriptome by high-throughput sequencing. Nat Genet. 2008; 40(12): 1413-1415. https://doi.org/10.1038/ng.259 PMID: 18978789

37. Kondrashov FA, Rogozin IB, Wolf YI, Koonin EV. Selection in the evolution of gene duplications. Genome Biol. 2002; 3(2): 1-9. https://doi.org/10.1186/gb-2002-3-2-research0008 PMID: 11864370

38. Esposito M, Moreno-Hagelsieb G. Non-synonymous to synonymous substitutions suggest that orthologs tend to keep their functions, while paralogs are a source of functional novelty. bioRxiv. 2018: 354704. https://doi.org/10.1101/354704

39. Guéguen L, Duret L. Unbiased estimate of synonymous and nonsynonymous substitution rates with nonstationary base composition. Mol Biol Evol. 2018; 35(3): 734-742. https://doi.org/10.1093/molbev/msx308 PMID: 29220511

40. Takata MA, Gonçalves-Carneiro D, Zang TM, Soll SJ, York A, Blanco-Melo D, et al. CG dinucleotide suppression enables antiviral defence targeting non-self RNA. Nature. 2017; 550(7674): 124-127. https://doi.org/10.1038/nature24039 PMID: 28953888

41. Sievers A, Bosiek K, Bisch M, Dreessen C, Riedel J, Froß P, et al. K-mer content, correlation, and position analysis of genome DNA sequences for the identification of function and evolutionary features. Genes. 2017; 8(4): 122. https://doi.org/10.3390/genes8040122 PMID: 28422050

1164 42. Yu C-H, Dang Y, Zhou Z, Wu C, Zhao F, Sachs MS, et al. Codon usage influences the local
1165 rate of translation elongation to regulate co-translational protein folding. Mol Cell. 2015; 59(5):
1166 744-754. https://doi.org/10.1016/j.molcel.2015.07.018 PMID: 26321254
1167 43. Zhou Z, Dang Y, Zhou M, Li L, Yu C-h, Fu J, et al. Codon usage is an important determinant
1168 of gene expression levels largely through its effects on transcription. Proceedings of the
1169 National Academy of Sciences. 2016; 113(41): E6117-E6125.
1170 https://doi.org/10.1073/pnas.1606724113 PMID: 27671647
1171 44. Pommié C, Levadoux S, Sabatier R, Lefranc G, Lefranc MP. IMGT standardized criteria for
1172 statistical analysis of immunoglobulin V-REGION amino acid properties. J Mol Recognit.
1173 2004; 17(1): 17-32. https://doi.org/10.1002/jmr.647 PMID: 14872534
1174 45. Kumar M, Gouw M, Michael S, Sámano-Sánchez H, Pancsa R, Glavina J, et al. ELM—the
1175 eukaryotic linear motif resource in 2020. Nucleic Acids Res. 2020; 48(D1): D296-D306.
1176 https://doi.org/10.1093/nar/gkz1030 PMID: 31680160
1177 46. Tufarelli C, Ahmad A, Strohbuecker S, Scotti C, Sottile V. In Silico Identification of SOX1
1178 Post-Translational Modifications Highlights a Shared Protein Motif. 2020.
1179 https://doi.org/10.3390/cells9112471 PMID: 33202879
1180 47. Alanis-Lobato G, Andrade-Navarro MA, Schaefer MH. HIPPIE v2.0: enhancing
1181 meaningfulness and reliability of protein–protein interaction networks. Nucleic Acids Res.
1182 2016: gkw985. https://doi.org/10.1093/nar/gkw985 PMID: 27794551
1183 48. Yoon J, Blumer A, Lee K. An algorithm for modularity analysis of directed and weighted
1184 biological networks based on edge-betweenness centrality. Bioinformatics. 2006; 22(24):
1185 3106-3108. https://doi.org/10.1093/bioinformatics/btl533 PMID: 17060356
1186 49. Friedel CC, Zimmer R. Influence of degree correlations on network structure and stability in
1187 protein-protein interaction networks. BMC Bioinformatics. 2007; 8(1): 1-10.
1188 https://doi.org/10.1186/1471-2105-8-297 PMID: 17688687
1189 50. Ravasz E, Somera AL, Mongru DA, Oltvai ZN, Barabási A-L. Hierarchical organization of
1190 modularity in metabolic networks. Science. 2002; 297(5586): 1551-1555.
1191 https://doi.org/10.1126/science.1073374 PMID: 12202830
1192 51. Hagai T, Azia A, Babu MM, Andino R. Use of host-like peptide motifs in viral proteins is a
1193 prevalent strategy in host-virus interactions. Cell Rep. 2014; 7(5): 1729-1739.
1194 https://doi.org/10.1016/j.celrep.2014.04.052 PMID: 24882001
1195 52. Noble WS. How does multiple testing correction work? Nat Biotechnol. 2009; 27(12): 1135-
1196 1137. https://doi.org/10.1038/nbt1209-1135 PMID: 20010596

53. Chang C-C, Lin C-J. LIBSVM: A library for support vector machines. ACM Trans Intell Syst Technol. 2011; 2(3): 1-27. https://doi.org/10.1145/1961189.1961199

54. Chicco D, Jurman G. The advantages of the Matthews correlation coefficient (MCC) over F1 score and accuracy in binary classification evaluation. BMC Genomics. 2020; 21(1): 1-13. https://doi.org/10.1186/s12864-019-6413-7 PMID: 31898477

55. MacFarland TW, Yates JM. Mann–whitney u test. Introduction to nonparametric statistics for the biological sciences using R: Springer; 2016. p. 103-132.

56. Van den Eynden J, Larsson E. Mutational signatures are critical for proper estimation of purifying selection pressures in cancer somatic mutation data when using the dN/dS metric. Front Genet. 2017; 8: 74. https://doi.org/10.3389/fgene.2017.00074 PMID: 28642787

57. Song H, Bremer BJ, Hinds EC, Raskutti G, Romero PA. Inferring protein sequence-function relationships with large-scale positive-unlabeled learning. Cell Syst. 2020. https://doi.org/10.1016/j.cels.2020.10.007 PMID: 33212013

58. Pessia E, Popa A, Mousset S, Rezvoy C, Duret L, Marais GA. Evidence for widespread GC-biased gene conversion in eukaryotes. Genome Biol Evol. 2012; 4(7): 675-682. https://doi.org/10.1093/gbe/evs052 PMID: 22628461

59. Lee NK, Li X, Wang D. A comprehensive survey on genetic algorithms for DNA motif prediction. Inf Sci. 2018; 466: 25-43. https://doi.org/10.1016/j.ins.2018.07.004

60. Di Rienzo L, Miotto M, Bò L, Ruocco G, Raimondo D, Milanetti E. Characterizing hydropathy of amino acid side chain in a protein environment by investigating the structural changes of water molecules network. Front Mol Biosci. 2021; 8. https://doi.org/10.3389/fmolb.2021.626837 PMID: 33718433

61. Bhadra P, Yan J, Li J, Fong S, Siu SW. AmPEP: Sequence-based prediction of antimicrobial peptides using distribution patterns of amino acid properties and random forest. Sci Rep. 2018; 8(1): 1-10. https://doi.org/10.1038/s41598-018-19752-w PMID: 29374199

62. Pfleger CM, Kirschner MW. The KEN box: an APC recognition signal distinct from the D box targeted by Cdh1. Genes Dev. 2000; 14(6): 655-665. PMID: 10733526

63. Fehr AR, Yu D. Control the host cell cycle: viral regulation of the anaphase-promoting complex. J Virol. 2013; 87(16): 8818-8825. https://doi.org/10.1128/JVI.00088-13 PMID: 23760246

64. Bösl K, Ianevski A, Than TT, Andersen PI, Kuivanen S, Teppor M, et al. Common nodes of virus–host interaction revealed through an integrated network analysis. Front Immunol. 2019; 10: 2186. https://doi.org/10.3389/fimmu.2019.02186 PMID: 31636628

65. Wright PE, Dyson HJ. Intrinsically disordered proteins in cellular signalling and regulation. Nat Rev Mol Cell Biol. 2015; 16(1): 18-29. https://doi.org/10.1038/nrm3920 PMID: 25531225

66. Mészáros B, Erdős G, Dosztányi Z. IUPred2A: context-dependent prediction of protein disorder as a function of redox state and protein binding. Nucleic Acids Res. 2018; 46(W1): W329-W337. https://doi.org/10.1093/nar/gky384 PMID: 29860432

67. Michael S, Travé G, Ramu C, Chica C, Gibson TJ. Discovery of candidate KEN-box motifs using cell cycle keyword enrichment combined with native disorder prediction and motif conservation. Bioinformatics. 2008; 24(4): 453-457. https://doi.org/10.1093/bioinformatics/btm624 PMID: 18184688

68. Abedi M, Gheisari Y. Nodes with high centrality in protein interaction networks are responsible for driving signaling pathways in diabetic nephropathy. PeerJ. 2015; 3: e1284. https://doi.org/10.7717/peerj.1284 PMID: 26557424

69. Ozato K, Shin D-M, Chang T-H, Morse HC. TRIM family proteins and their emerging roles in innate immunity. Nat Rev Immunol. 2008; 8(11): 849-860. https://doi.org/10.1038/nri2413

70. Shaw AE, Rihn SJ, Mollentze N, Wickenhagen A, Stewart DG, Orton RJ, et al. The antiviral state has shaped the CpG composition of the vertebrate interferome to avoid self-targeting. PLoS Biol. 2021; 19(9): e3001352. https://doi.org/10.1371/journal.pbio.3001352 PMID: 34491982

71. Yeom S, Giacomelli I, Fredrikson M, Jha S, editors. Privacy risk in machine learning: Analyzing the connection to overfitting. 2018 IEEE 31st Computer Security Foundations Symposium (CSF); 2018: IEEE.

72. Ali J, Khan R, Ahmad N, Maqsood I. Random forests and decision trees. International Journal of Computer Science Issues (IJCSI). 2012; 9(5): 272.

73. Zhang M-L, Zhou Z-H. ML-KNN: A lazy learning approach to multi-label learning. Pattern recognition. 2007; 40(7): 2038-2048. https://doi.org/10.1016/j.patcog.2006.12.019

74. Cheng D, Zhang S, Deng Z, Zhu Y, Zong M, editors. kNN algorithm with data-driven k value. International Conference on Advanced Data Mining and Applications; 2014: Springer.

75. Zhang J, Chai H, Gao B, Yang G, Ma Z. HEMEsPred: Structure-based ligand-specific heme binding residues prediction by using fast-adaptive ensemble learning scheme. IEEE/ACM Trans Comput Biol Bioinform. 2016; 15(1): 147-156. https://doi.org/10.1109/TCBB.2016.2615010 PMID: 28029626

76. Lonsdale J, Thomas J, Salvatore M, Phillips R, Lo E, Shad S, et al. The genotype-tissue expression (GTEx) project. Nat Genet. 2013; 45(6): 580-585. https://doi.org/10.1038/ng.2653

77. Papatheodorou I, Moreno P, Manning J, Fuentes AM-P, George N, Fexova S, et al. Expression Atlas update: from tissues to single cells. Nucleic Acids Res. 2020; 48(D1): D77-D83. https://doi.org/10.1093/nar/gkz947 PMID: 31665515

78. Jeong H, Mason SP, Barabási A-L, Oltvai ZN. Lethality and centrality in protein networks. Nature. 2001; 411(6833): 41-42. https://doi.org/10.1038/35075138 PMID: 11333967

79. Hahn MW, Kern AD. Comparative genomics of centrality and essentiality in three eukaryotic protein-interaction networks. Mol Biol Evol. 2005; 22(4): 803-806. https://doi.org/10.1093/molbev/msi072 PMID: 15616139

80. Batada NN, Hurst LD, Tyers M. Evolutionary and physiological importance of hub proteins. PLoS Comput Biol. 2006; 2(7): e88. https://doi.org/10.1371/journal.pcbi.0020088 PMID: 16839197

81. Pérez-Martínez D. Innate immunity in vertebrates: an overview. Immunology. 2016; 148(2): 125-139. https://doi.org/10.1111/imm.12597 PMID: 26878338

82. Jopling CL. Mutations: Stop that nonsense! Elife. 2014; 3: e04300. https://doi.org/10.7554/eLife.04300

83. Zhu X, Pribis JP, Rodriguez PC, Morris Jr SM, Vodovotz Y, Billiar TR, et al. The central role of arginine catabolism in T-cell dysfunction and increased susceptibility to infection after physical injury. Ann Surg. 2014; 259(1): 171-178. https://doi.org/10.1097/SLA.0b013e31828611f8 PMID: 23470573

84. Morris CR, Hamilton-Reeves J, Martindale RG, Sarav M, Ochoa Gautier JB. Acquired amino acid deficiencies: a focus on arginine and glutamine. Nutr Clin Pract. 2017; 32: 30S-47S. https://doi.org/10.1177/0884533617691250 PMID: 28388380

85. Levring TB, Hansen AK, Nielsen BL, Kongsbak M, Von Essen MR, Woetmann A, et al. Activated human CD4+ T cells express transporters for both cysteine and cystine. Sci Rep. 2012; 2(1): 1-6. https://doi.org/10.1038/srep00266 PMID: 22355778

86. Sikalidis AK. Amino acids and immune response: a role for cysteine, glutamine, phenylalanine, tryptophan and arginine in T-cell function and cancer? Pathol Oncol Res. 2015; 21(1): 9-17. https://doi.org/10.1007/s12253-014-9860-0 PMID: 25351939

87. Yin C, Zheng T, Chang X. Biosynthesis of S-Adenosylmethionine by magnetically immobilized Escherichia coli cells highly expressing a methionine adenosyltransferase variant. Molecules. 2017; 22(8): 1365. https://doi.org/10.3390/molecules22081365 PMID: 28820476

88. Feld JJ, Modi AA, El–Diwany R, Rotman Y, Thomas E, Ahlenstiel G, et al. S-adenosyl methionine improves early viral responses and interferon-stimulated gene induction in hepatitis

C nonresponders. Gastroenterology. 2011; 140(3): 830-839. https://doi.org/10.1053/j.gastro.2010.09.010 PMID: 20854821

89. Li S-W, Lai C-C, Ping J-F, Tsai F-J, Wan L, Lin Y-J, et al. Severe acute respiratory syndrome coronavirus papain-like protease suppressed alpha interferon-induced responses through downregulation of extracellular signal-regulated kinase 1-mediated signalling pathways. J Gen Virol. 2011; 92(5): 1127-1140. https://doi.org/10.1099/vir.0.028936-0 PMID: 21270289

90. Flo TH, Smith KD, Sato S, Rodriguez DJ, Holmes MA, Strong RK, et al. Lipocalin 2 mediates an innate immune response to bacterial infection by sequestrating iron. Nature. 2004; 432(7019): 917-921. https://doi.org/10.1038/nature03104 PMID: 15531878

91. Noçon AL, Ip JP, Terry R, Lim SL, Getts DR, Müller M, et al. The bacteriostatic protein lipocalin 2 is induced in the central nervous system of mice with West Nile virus encephalitis. J Virol. 2014; 88(1): 679-689. https://doi.org/10.1128/JVI.02094-13 PMID: 24173226

92. Tissot C, Rebouissou C, Klein B, Mechti N. Both human α/β and γ interferons upregulate the expression of CD48 cell surface molecules. J Interferon Cytokine Res. 1997; 17(1): 17-26. https://doi.org/10.1089/jir.1997.17.17 PMID: 9041467

93. Zarama A, Perez-Carmona N, Farre D, Tomic A, Borst EM, Messerle M, et al. Cytomegalovirus m154 hinders CD48 cell-surface expression and promotes viral escape from host natural killer cell control. PLoS Pathog. 2014; 10(3): e1004000. https://doi.org/10.1371/journal.ppat.1004000 PMID: 24626474

94. Martínez-Vicente P, Farré D, Engel P, Angulo A. Divergent Traits and Ligand-Binding Properties of the Cytomegalovirus CD48 Gene Family. Viruses. 2020; 12(8): 813. https://doi.org/10.3390/v12080813 PMID: 32731344

95. Ricquier D. UCP1, the mitochondrial uncoupling protein of brown adipocyte: a personal contribution and a historical perspective. Biochimie. 2017; 134: 3-8. https://doi.org/10.1016/j.biochi.2016.10.018 PMID: 27916641

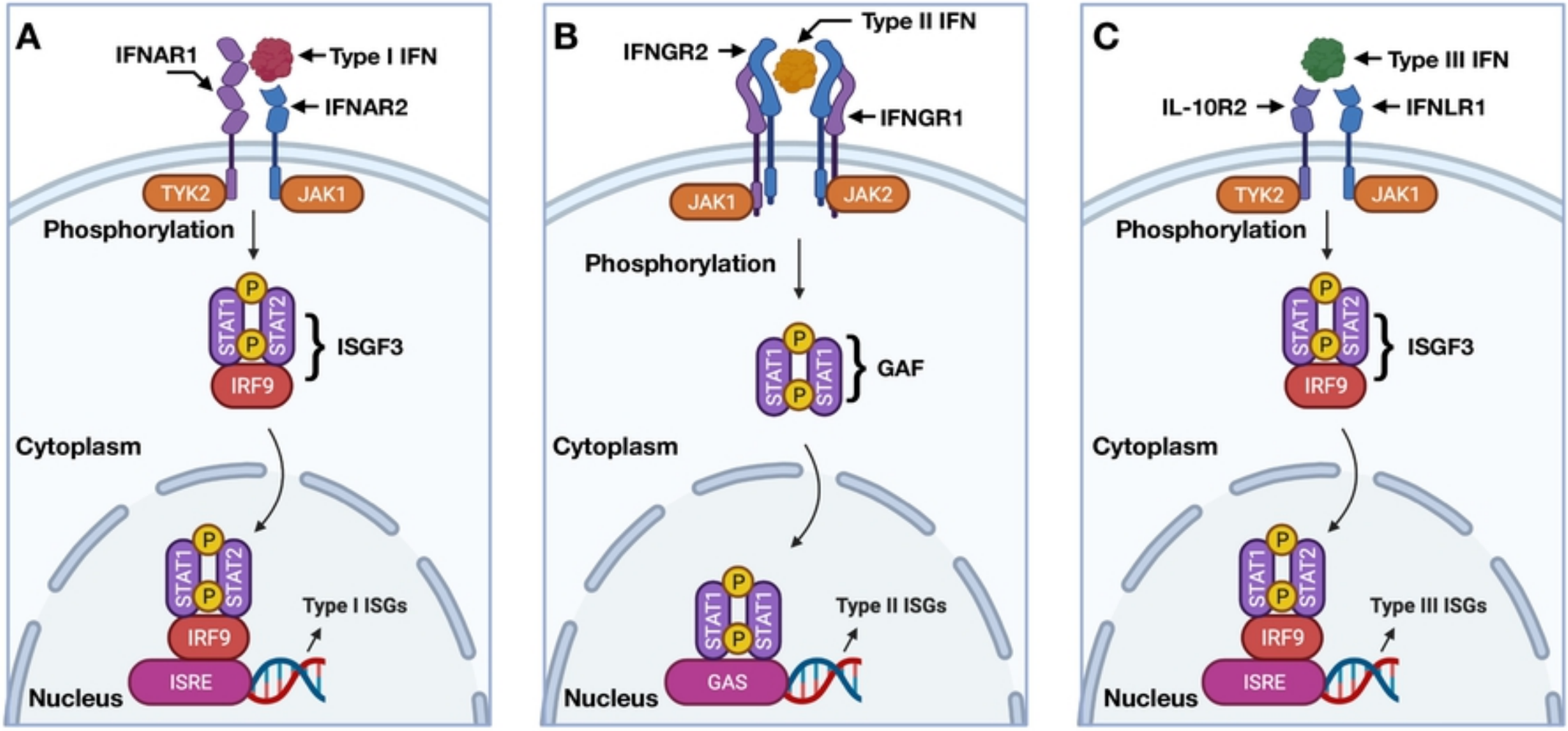
A
IFNAR1
Type I IFN
IFNAR2
TYK2
JAK1
Phosphorylation
P
STAT1
STAT2
P
ISGF3
IRF9
Cytoplasm
P
STAT1
STAT2
P
IRF9
Type I ISGs
ISRE
Nucleus
B
Type II IFN
IFNGR2
IFNGR1
JAK1
JAK2
Phosphorylation
P
STAT1
STAT1
P
GAF
Cytoplasm
P
STAT1
STAT1
P
Type II ISGs
GAS
Nucleus
C
Type III IFN
IL-10R2
IFNLR1
TYK2
JAK1
Phosphorylation
P
STAT1
STAT2
P
ISGF3
IRF9
Cytoplasm
P
STAT1
STAT2
P
IRF9
Type III ISGs
ISRE
Nucleus

Figure 1

BEGIN

Initialisation: Balanced dataset $S_0 = \{(1, v_1^0), .. (1, v_n^0), (0, v_{n+1}^0) ... (0, v_{2n}^0)\}$, dimension of the feature vector D_0, machine learning algorithm A, number of disruptive feature $d_0 = D_0$, and iteration round $i = 0$.

While $d_0 > 0$ (i^{th} iteration):

1) Use five-fold cross validation on dataset S_i, prediction $P_i = A(S_i)$;
2) Evaluate the P_i with the criterion of AUC;
3) Remove one feature from feature vector v^i and generate a temporary dataset T_i;
4) Use five-fold cross validation on dataset T_i, prediction $P'_i = A(T_i)$;
5) Evaluate the P'_i with the criterion of AUC;
6) Repeat 4) and 5) for the traversal of D_i features;
7) Traverse v^i and remove m features helpful to improve AUC of P'_i, $d_i = m$;
8) Update dataset $S_{i+1} = \{(1, v_1^{i+1}), .. (1, v_n^{i+1}), (0, v_{n+1}^{i+1}) ... (0, v_{2n}^{i+1})\}$, $D_{i+1} = D_i - m$.

End

Output: dataset S_{i-1} encoded by D_{i-1} features.

END

Figure 2

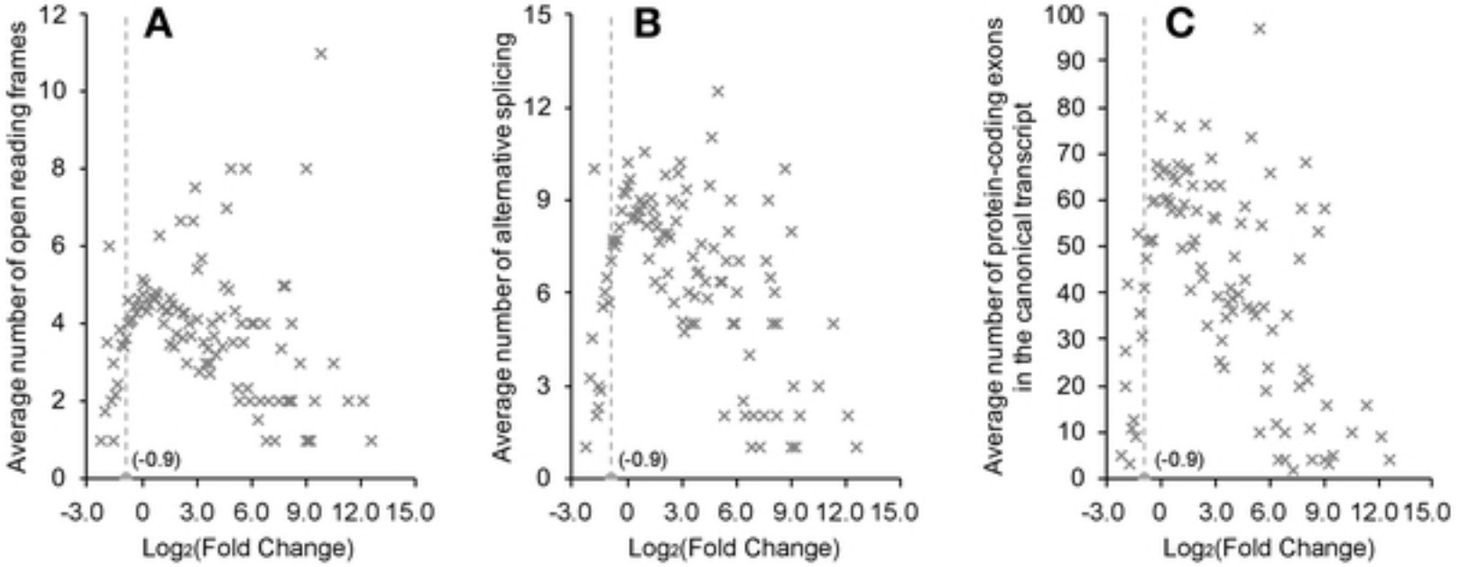
A
Average number of open reading frames
(-0.9)
Log2(Fold Change)
B
Average number of alternative splicing
(-0.9)
Log2(Fold Change)
C
Average number of protein-coding exons in the canonical transcript
(-0.9)
Log2(Fold Change)

Figure 3

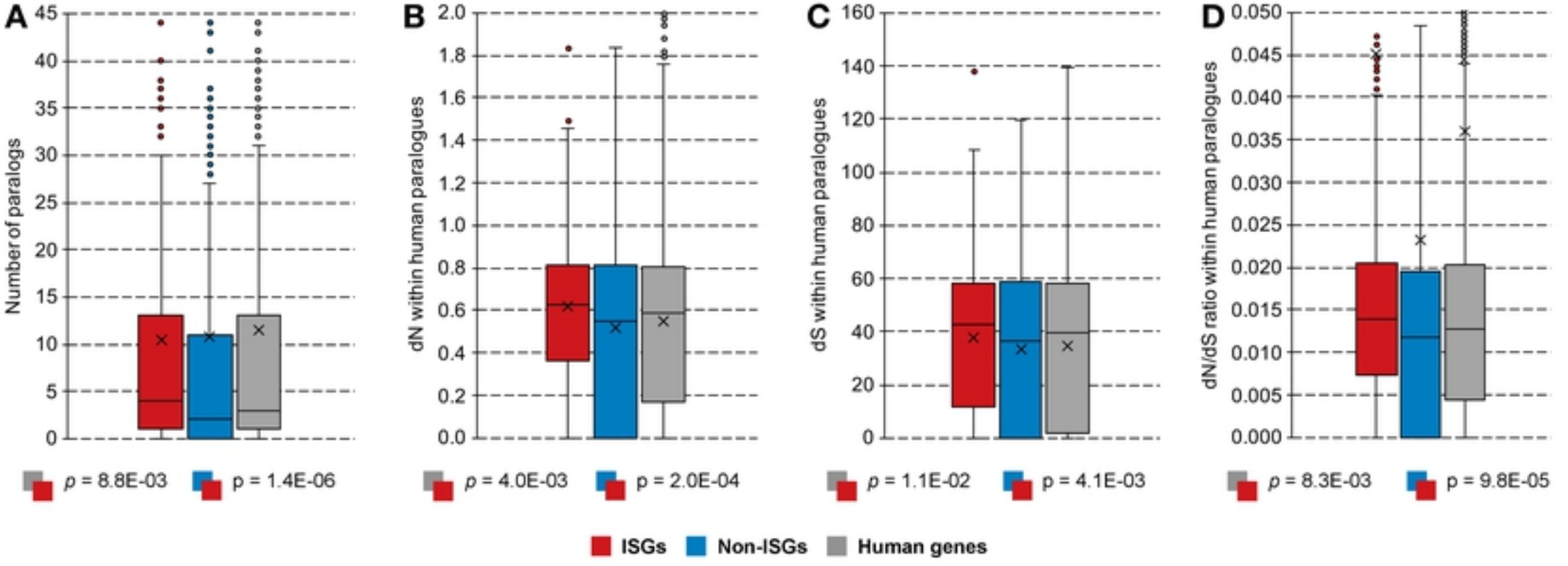
A
Number of paralogs
p = 8.8E-03
p = 1.4E-06
B
dN within human paralogues
p = 4.0E-03
p = 2.0E-04
C
dS within human paralogues
p = 1.1E-02
p = 4.1E-03
D
dN/dS ratio within human paralogues
p = 8.3E-03
p = 9.8E-05
ISGs
Non-ISGs
Human genes

Figure 4

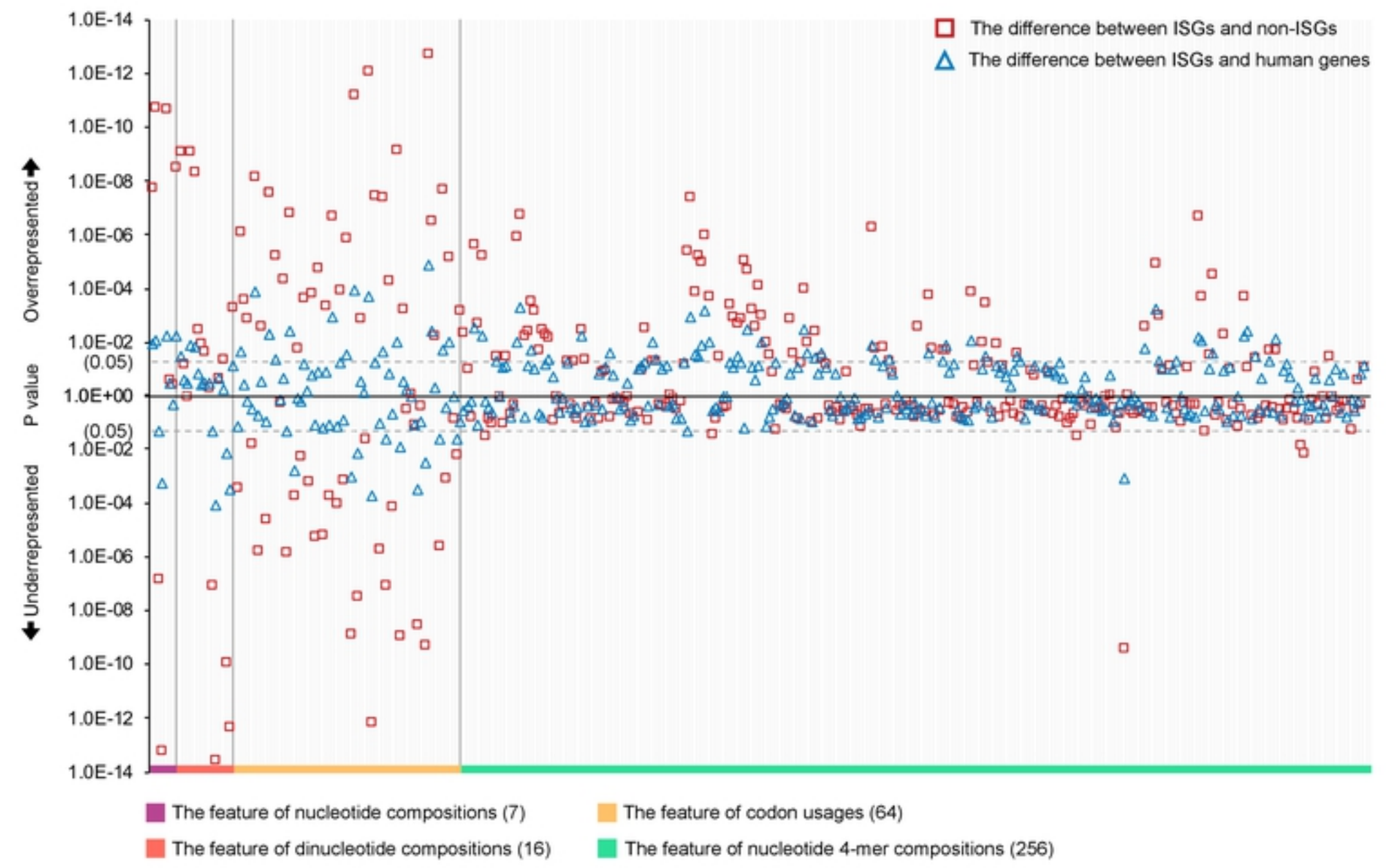
The difference between ISGs and non-ISGs
The difference between ISGs and human genes
Overrepresented
P value
Underrepresented
1.0E-14
1.0E-12
1.0E-10
1.0E-08
1.0E-06
1.0E-04
1.0E-02
(0.05)
1.0E+00
(0.05)
1.0E-02
1.0E-04
1.0E-06
1.0E-08
1.0E-10
1.0E-12
1.0E-14
The feature of nucleotide compositions (7)
The feature of codon usages (64)
The feature of dinucleotide compositions (16)
The feature of nucleotide 4-mer compositions (256)

Figure 5

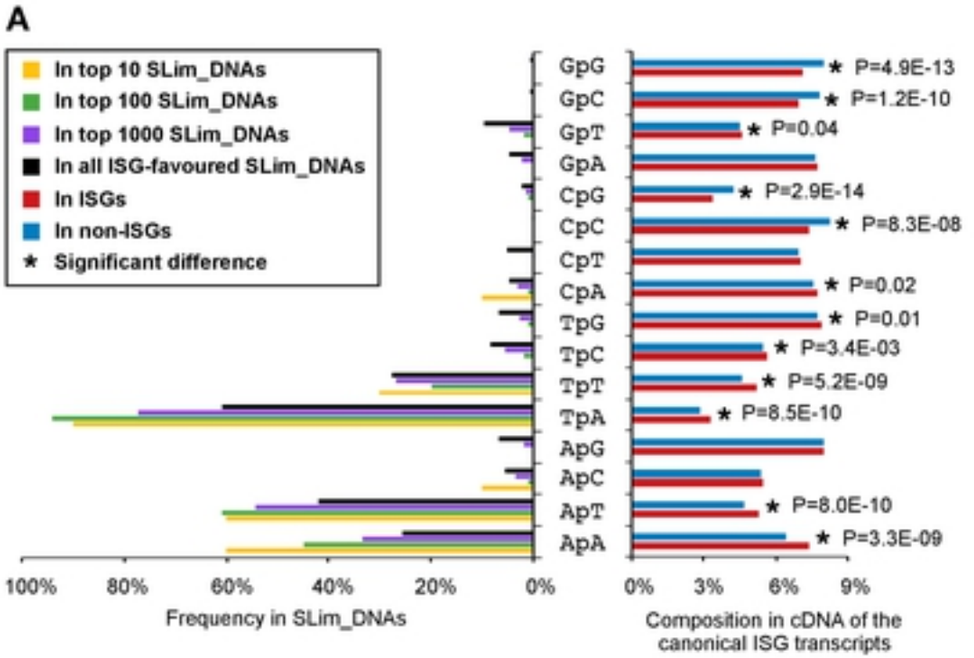
A
In top 10 SLim_DNAs
In top 100 SLim_DNAs
In top 1000 SLim_DNAs
In all ISG-favoured SLim_DNAs
In ISGs
In non-ISGs
Significant difference
GpG
GpC
GpT
GpA
CpG
CpC
CpT
CpA
TpG
TpC
TpT
TpA
ApG
ApC
ApT
ApA
P=4.9E-13
P=1.2E-10
P=0.04
P=2.9E-14
P=8.3E-08
P=0.02
P=0.01
P=3.4E-03
P=5.2E-09
P=8.5E-10
P=8.0E-10
P=3.3E-09
100% 80% 60% 40% 20% 0%
Frequency in SLim_DNAs
0% 3% 6% 9%
Composition in cDNA of the canonical ISG transcripts

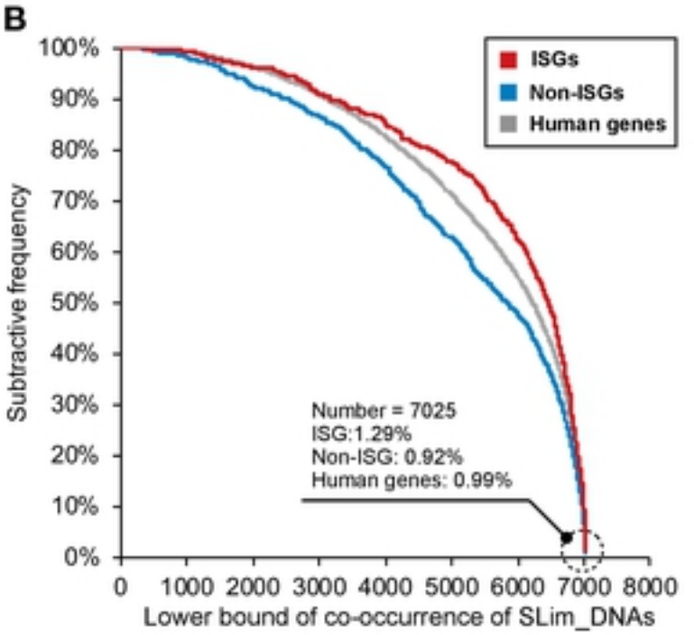
B
ISGs
Non-ISGs
Human genes
Subtractive frequency
100%
90%
80%
70%
60%
50%
40%
30%
20%
10%
0%
Number = 7025
ISG:1.29%
Non-ISG: 0.92%
Human genes: 0.99%
0 1000 2000 3000 4000 5000 6000 7000 8000
Lower bound of co-occurrence of SLim_DNAs

Figure 6

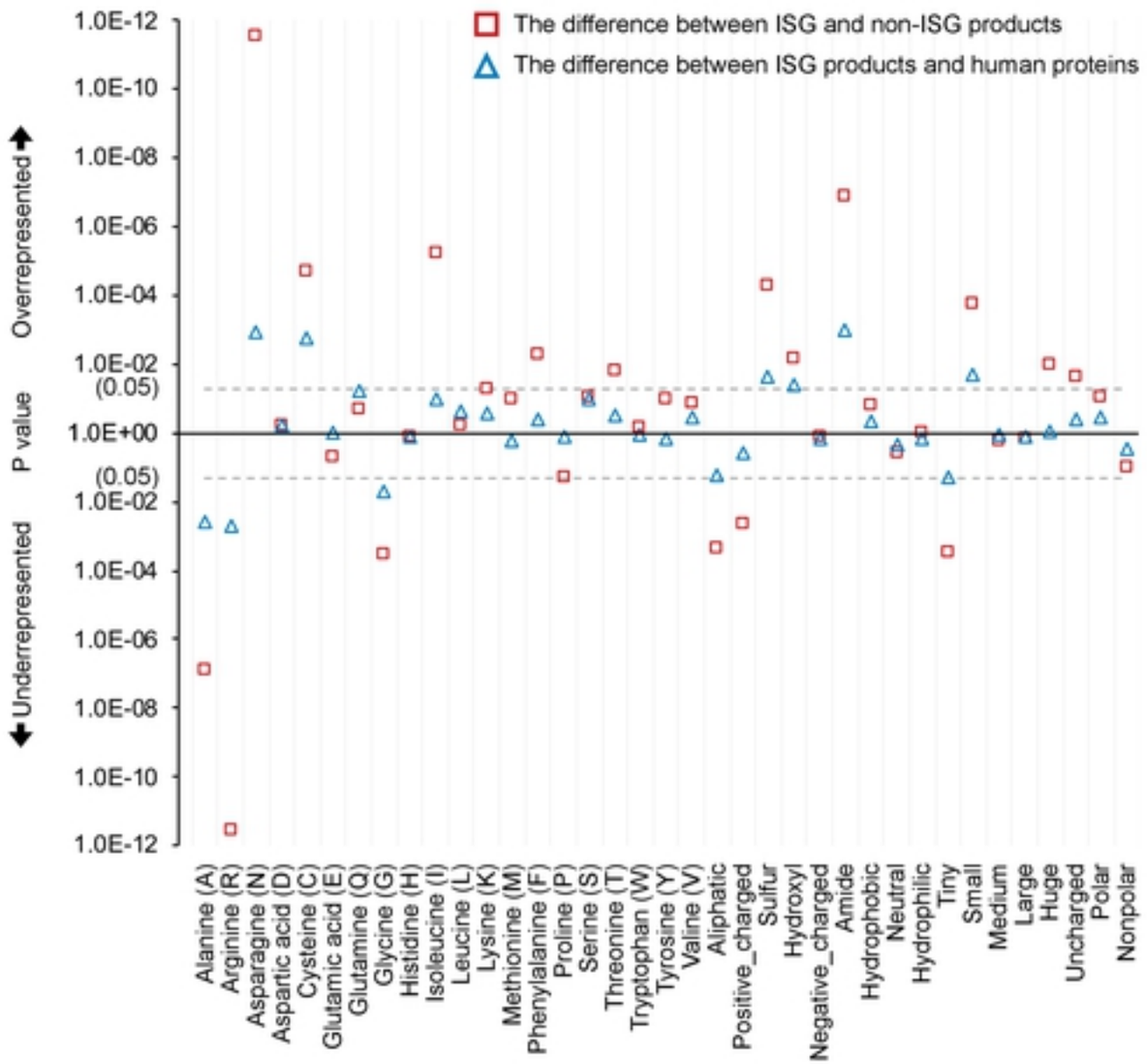
The difference between ISG and non-ISG products
The difference between ISG products and human proteins
Overrepresented
P value
Underrepresented
1.0E-12
1.0E-10
1.0E-08
1.0E-06
1.0E-04
1.0E-02
(0.05)
1.0E+00
(0.05)
1.0E-02
1.0E-04
1.0E-06
1.0E-08
1.0E-10
1.0E-12
Alanine (A)
Arginine (R)
Asparagine (N)
Aspartic acid (D)
Cysteine (C)
Glutamic acid (E)
Glutamine (Q)
Glycine (G)
Histidine (H)
Isoleucine (I)
Leucine (L)
Lysine (K)
Methionine (M)
Phenylalanine (F)
Proline (P)
Serine (S)
Threonine (T)
Tryptophan (W)
Tyrosine (Y)
Valine (V)
Aliphatic
Positive_charged
Sulfur
Hydroxyl
Negative_charged
Amide
Hydrophobic
Neutral
Hydrophilic
Tiny
Small
Medium
Large
Huge
Uncharged
Polar
Nonpolar

Figure 7

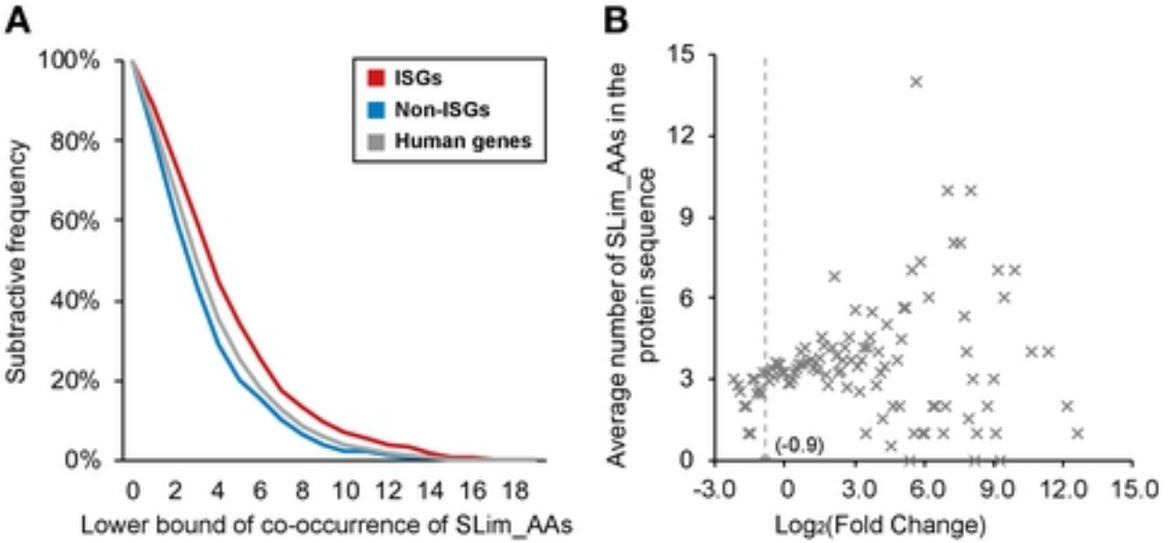
A
100%
80%
60%
40%
20%
0%
Subtractive frequency
0 2 4 6 8 10 12 14 16 18
Lower bound of co-occurrence of SLim_AAs
ISGs
Non-ISGs
Human genes
B
15
12
9
6
3
0
Average number of SLim_AAs in the protein sequence
(-0.9)
-3.0 0 3.0 6.0 9.0 12.0 15.0
Log2(Fold Change)

Figure 8

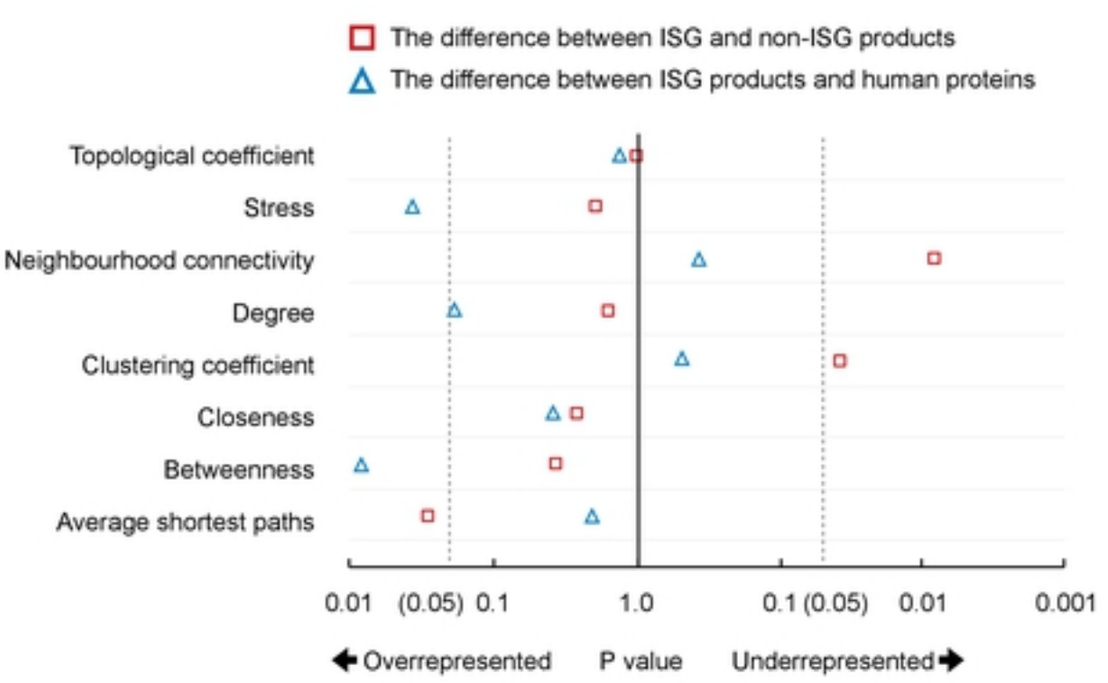
The difference between ISG and non-ISG products
The difference between ISG products and human proteins
Topological coefficient
Stress
Neighbourhood connectivity
Degree
Clustering coefficient
Closeness
Betweenness
Average shortest paths
0.01
(0.05)
0.1
1.0
0.1
(0.05)
0.01
0.001
Overrepresented
P value
Underrepresented

Figure 9

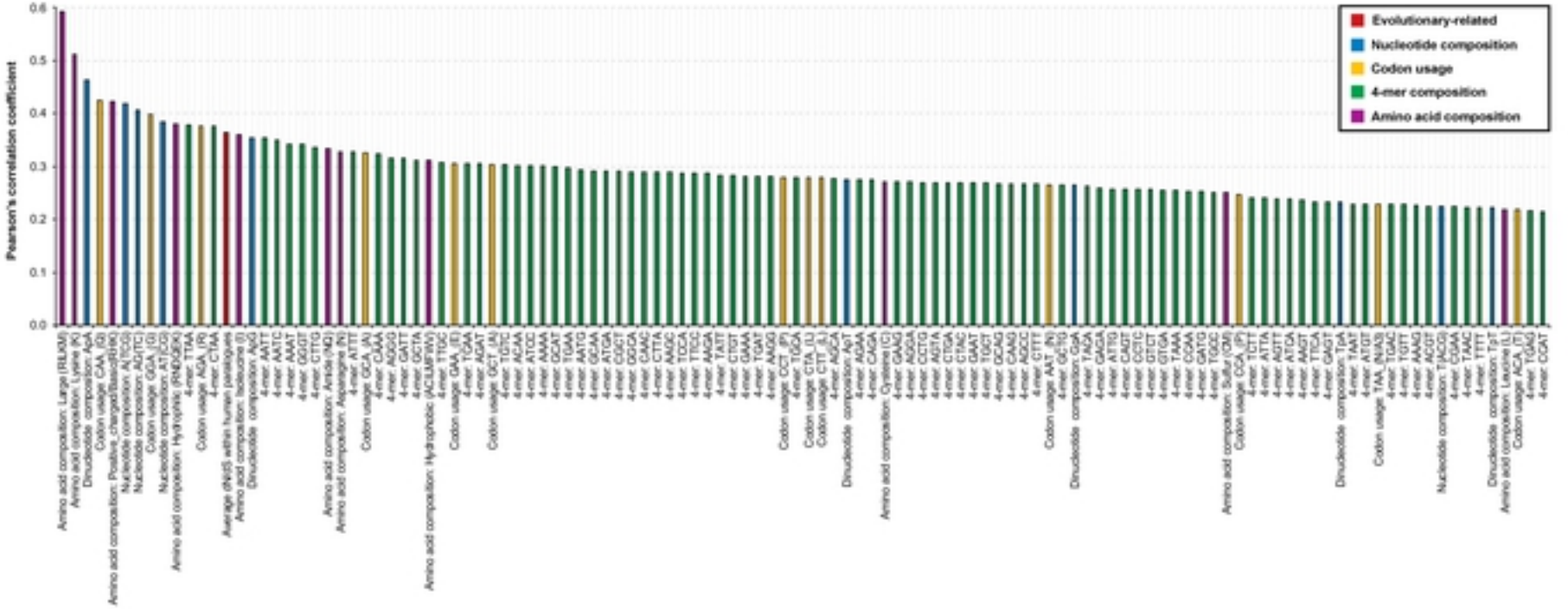
Pearson's correlation coefficient
0.0
0.1
0.2
0.3
0.4
0.5
0.6
Evolutionary-related
Nucleotide composition
Codon usage
4-mer composition
Amino acid composition
Amino acid composition: Large (RLKM)
Amino acid composition: Lysine (K)
Dinucleotide composition: ApA
Codon usage: CAA_(Q)
Amino acid composition: Positive_charged/Basic(RHK)
Nucleotide composition: A(TC)
Nucleotide composition: AG(TC)
Codon usage: GGA_(G)
Nucleotide composition: AT(CG)
Amino acid composition: Hydrophilic (RHDSEK)
4-mer: TTAA
Codon usage: AGA_(R)
4-mer: CTAA
Average dN/dS within human paralogues
Amino acid composition: Isoleucine (I)
Dinucleotide composition: ApG
4-mer: AATT
4-mer: AATC
4-mer: AAAT
4-mer: GGGT
4-mer: CTTG
Amino acid composition: Amide (NQ)
Amino acid composition: Asparagine (N)
4-mer: ATTT
Codon usage: GCA_(A)
4-mer: CAAA
4-mer: AGAG
4-mer: GATT
4-mer: GCTA
Amino acid composition: Hydrophobic (ACILMFWV)
4-mer: TTGC
Codon usage: GAA_(E)
4-mer: TGAA
4-mer: AGAT
Codon usage: GCT_(A)
4-mer: TGTC
4-mer: ACAA
4-mer: ATCC
4-mer: AAAA
4-mer: GCAT
4-mer: TGAA
4-mer: AATG
4-mer: GCAA
4-mer: ATGA
4-mer: CGCT
4-mer: GGCA
4-mer: CAAC
4-mer: CTTA
4-mer: AAGC
4-mer: TCCA
4-mer: TTCC
4-mer: AAGA
4-mer: TATT
4-mer: CTGT
4-mer: GAAA
4-mer: TGAT
4-mer: AAGG
Codon usage: CCT_(P)
4-mer: TGCA
Codon usage: CTA_(L)
Codon usage: CTT_(L)
4-mer: AGCA
Dinucleotide composition: ApT
4-mer: AGAA
4-mer: CAGA
Amino acid composition: Cysteine (C)
4-mer: GAAG
4-mer: AGGA
4-mer: CCTG
4-mer: AGTA
4-mer: CTGA
4-mer: CTAC
4-mer: GAAT
4-mer: TGCT
4-mer: GCAG
4-mer: CAAG
4-mer: ACCC
4-mer: GTTT
Codon usage: AAT_(N)
4-mer: GCTG
Dinucleotide composition: GpA
4-mer: TAGA
4-mer: GAGA
4-mer: ATTG
4-mer: CAGT
4-mer: CCTC
4-mer: GTCT
4-mer: GTGA
4-mer: TAAA
4-mer: CCAA
4-mer: GATG
4-mer: TGGC
Amino acid composition: Sulfur (GM)
Codon usage: CCA_(P)
4-mer: TCTT
4-mer: ATTA
4-mer: AGTT
4-mer: ATGA
4-mer: AAGT
4-mer: TTCA
4-mer: GAGT
Dinucleotide composition: TpA
4-mer: TAAT
4-mer: ATGT
Codon usage: TAA_(NAS)
4-mer: TGAC
4-mer: TGTT
4-mer: AAAG
4-mer: ACGT
Nucleotide composition: T(ACG)
4-mer: CGAA
4-mer: TAAC
4-mer: TTTT
Dinucleotide composition: TpT
Amino acid composition: Leucine (L)
Codon usage: ACA_(T)
4-mer: TGAG
4-mer: CCAT

Figure 10

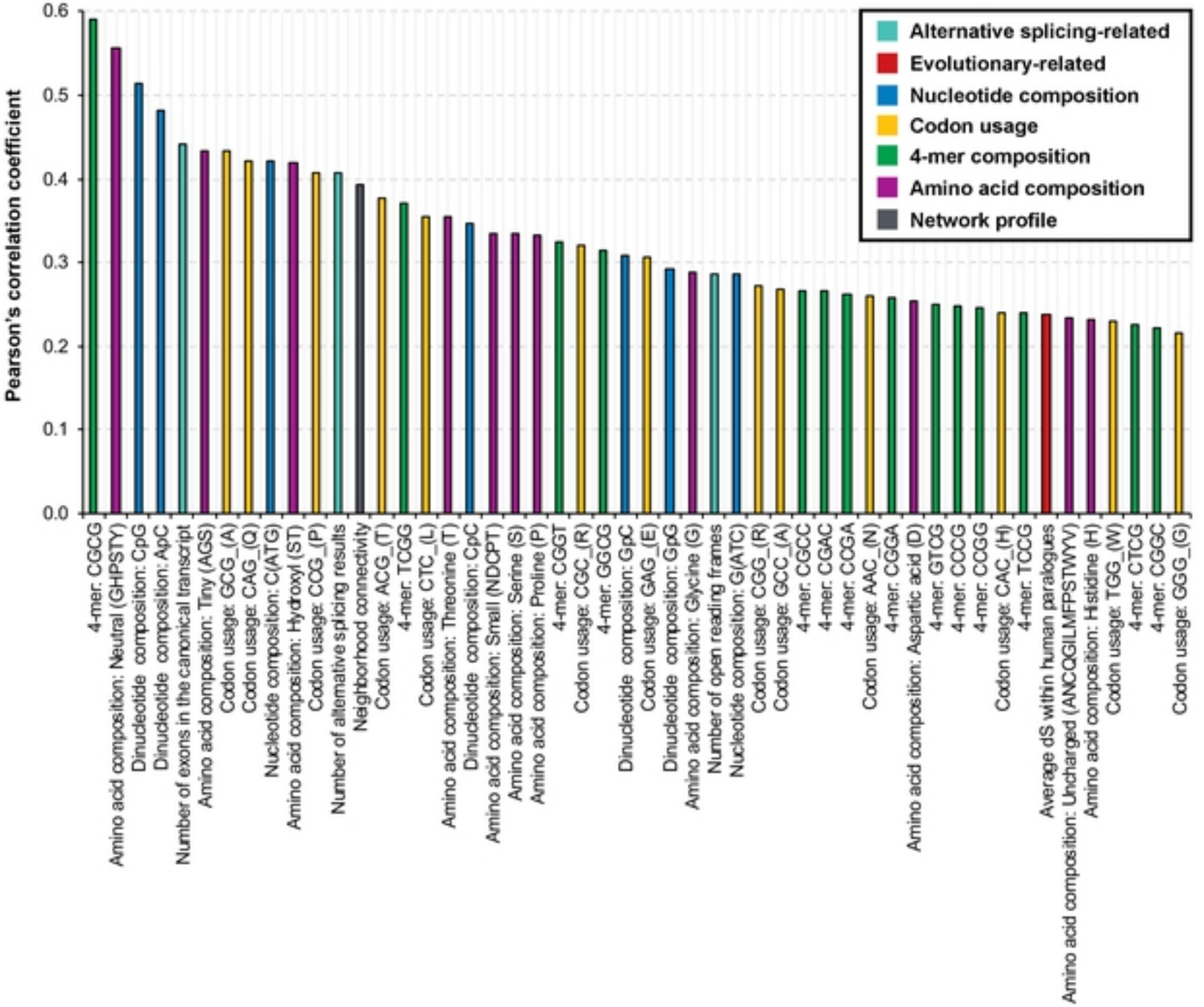
Pearson's correlation coefficient
0.0
0.1
0.2
0.3
0.4
0.5
0.6
Alternative splicing-related
Evolutionary-related
Nucleotide composition
Codon usage
4-mer composition
Amino acid composition
Network profile
4-mer: CGCG
Amino acid composition: Neutral (GHPSTY)
Dinucleotide composition: CpG
Dinucleotide composition: ApC
Number of exons in the canonical transcript
Amino acid composition: Tiny (AGS)
Codon usage: GCG_(A)
Codon usage: CAG_(Q)
Nucleotide composition: C(ATG)
Amino acid composition: Hydroxyl (ST)
Codon usage: CCG_(P)
Number of alternative splicing results
Neighborhood connectivity
Codon usage: ACG_(T)
4-mer: TCGG
Codon usage: CTC_(L)
Amino acid composition: Threonine (T)
Dinucleotide composition: CpC
Amino acid composition: Small (NDCPT)
Amino acid composition: Serine (S)
Amino acid composition: Proline (P)
4-mer: CGGT
Codon usage: CGC_(R)
4-mer: GGCG
Dinucleotide composition: GpC
Codon usage: GAG_(E)
Dinucleotide composition: GpG
Amino acid composition: Glycine (G)
Number of open reading frames
Nucleotide composition: G(ATC)
Codon usage: CGG_(R)
Codon usage: GCC_(A)
4-mer: CGCC
4-mer: CGAC
4-mer: CCGA
Codon usage: AAC_(N)
4-mer: CGGA
Amino acid composition: Aspartic acid (D)
4-mer: GTCG
4-mer: CCCG
4-mer: CCGG
Codon usage: CAC_(H)
4-mer: TCCG
Average dS within human paralogues
Amino acid composition: Uncharged (ANCQGILMFPSTWYV)
Amino acid composition: Histidine (H)
Codon usage: TGG_(W)
4-mer: CTCG
4-mer: CGGC
Codon usage: GGG_(G)

Figure 11

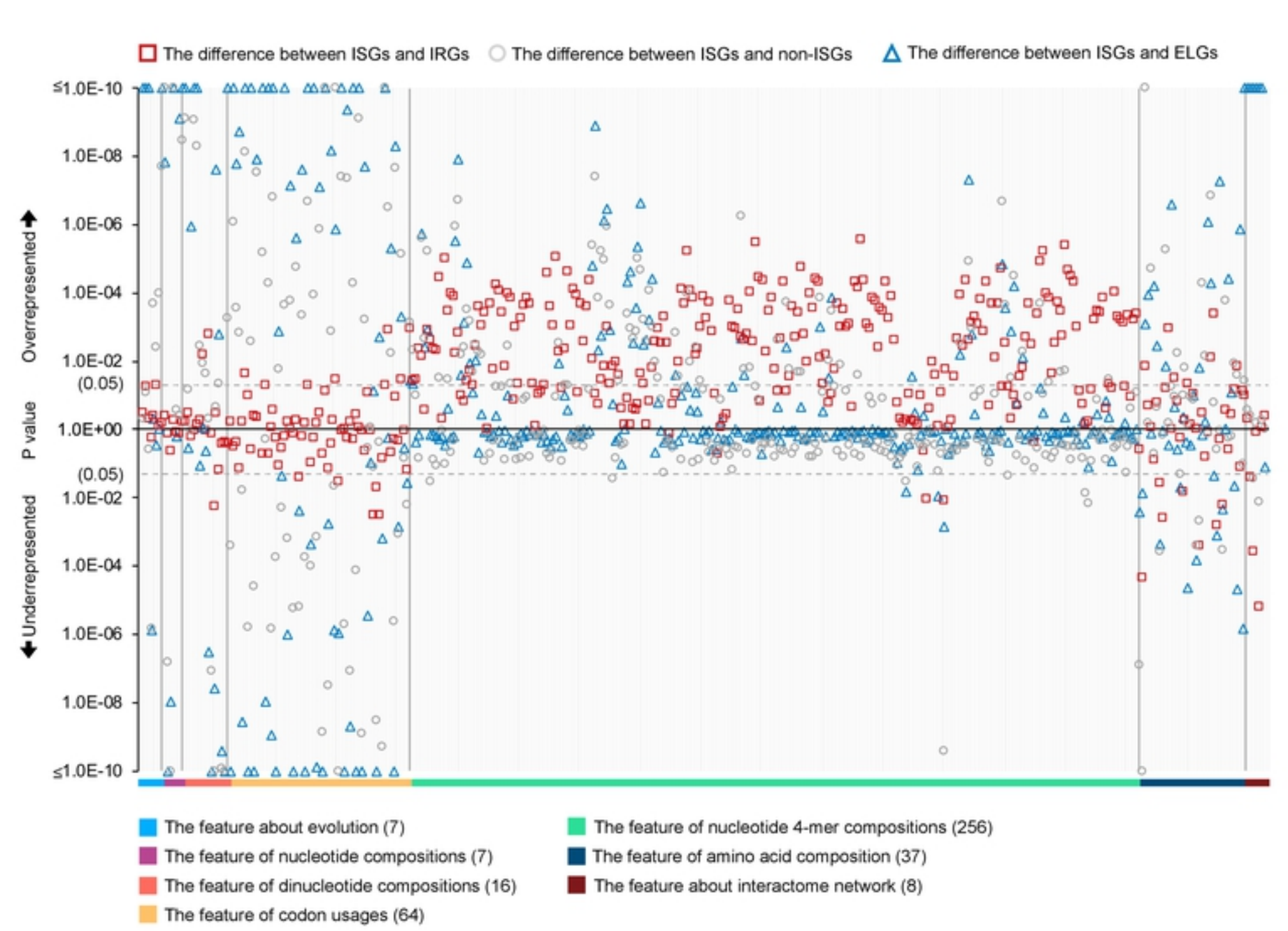
The difference between ISGs and IRGs
The difference between ISGs and non-ISGs
The difference between ISGs and ELGs
≤1.0E-10
1.0E-08
1.0E-06
1.0E-04
1.0E-02
(0.05)
1.0E+00
(0.05)
1.0E-02
1.0E-04
1.0E-06
1.0E-08
≤1.0E-10
Overrepresented
P value
Underrepresented
The feature about evolution (7)
The feature of nucleotide compositions (7)
The feature of dinucleotide compositions (16)
The feature of codon usages (64)
The feature of nucleotide 4-mer compositions (256)
The feature of amino acid composition (37)
The feature about interactome network (8)

Figure 12

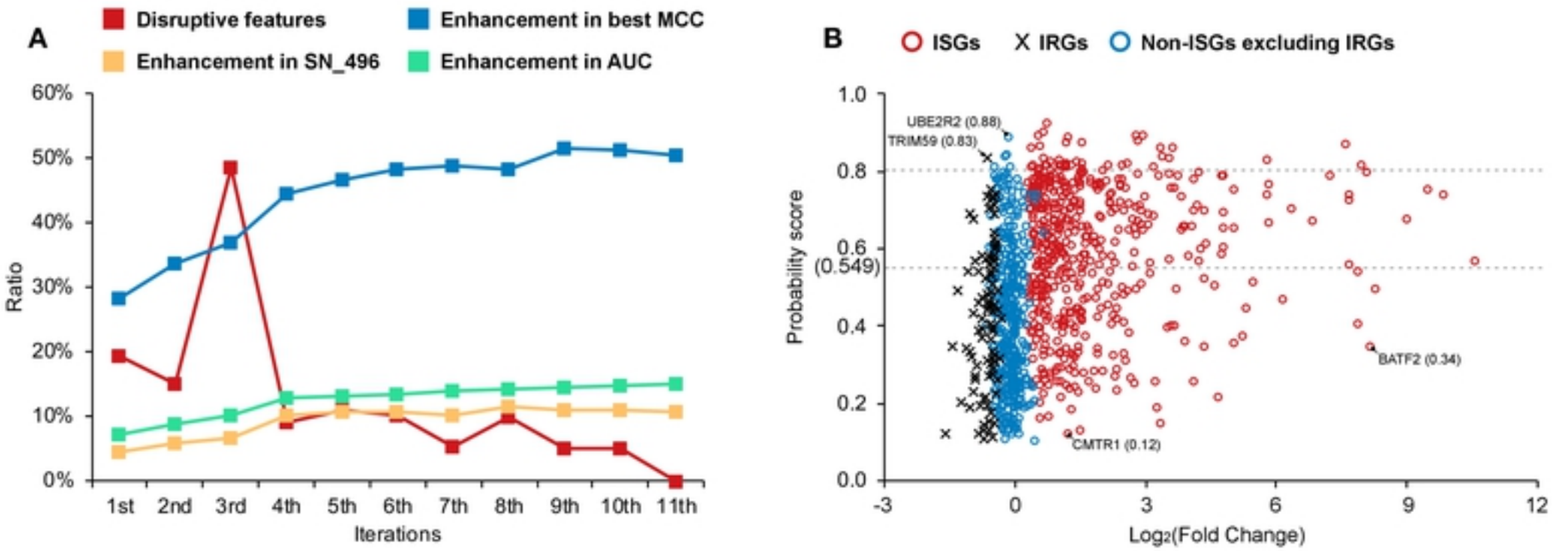
A
Disruptive features
Enhancement in best MCC
Enhancement in SN_496
Enhancement in AUC
60%
50%
40%
30%
20%
10%
0%
Ratio
1st
2nd
3rd
4th
5th
6th
7th
8th
9th
10th
11th
Iterations
B
ISGs
IRGs
Non-ISGs excluding IRGs
1.0
0.8
0.6
(0.549)
0.4
0.2
0.0
Probability score
UBE2R2 (0.88)
TRIM59 (0.83)
BATF2 (0.34)
CMTR1 (0.12)
-3
0
3
6
9
12
Log2(Fold Change)

Figure 13

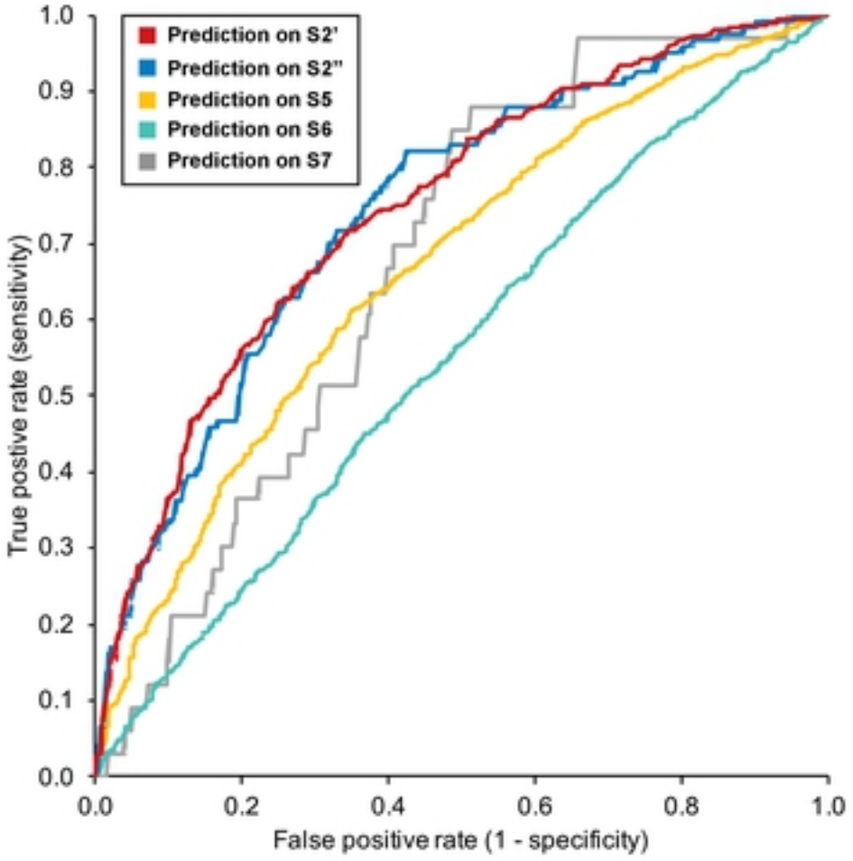
Prediction on S2'
Prediction on S2"
Prediction on S5
Prediction on S6
Prediction on S7
True postive rate (sensitivity)
False positive rate (1 - specificity)
0.0
0.1
0.2
0.3
0.4
0.5
0.6
0.7
0.8
0.9
1.0

Figure 14

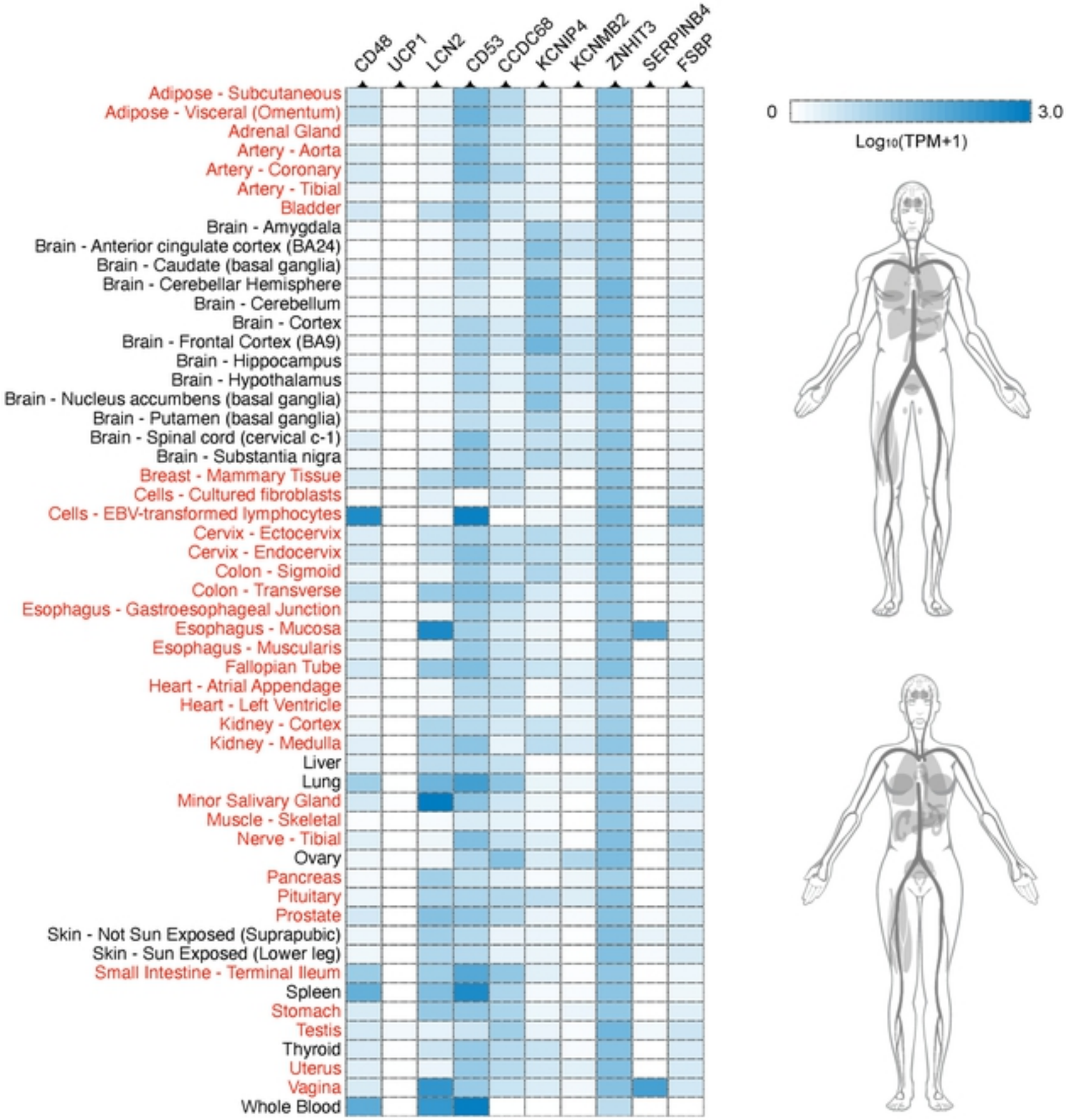
CD48
UCP1
LCN2
CD53
CCDC68
KCNIP4
KCNMB2
ZNHIT3
SERPINB4
FSBP
Adipose - Subcutaneous
Adipose - Visceral (Omentum)
Adrenal Gland
Artery - Aorta
Artery - Coronary
Artery - Tibial
Bladder
Brain - Amygdala
Brain - Anterior cingulate cortex (BA24)
Brain - Caudate (basal ganglia)
Brain - Cerebellar Hemisphere
Brain - Cerebellum
Brain - Cortex
Brain - Frontal Cortex (BA9)
Brain - Hippocampus
Brain - Hypothalamus
Brain - Nucleus accumbens (basal ganglia)
Brain - Putamen (basal ganglia)
Brain - Spinal cord (cervical c-1)
Brain - Substantia nigra
Breast - Mammary Tissue
Cells - Cultured fibroblasts
Cells - EBV-transformed lymphocytes
Cervix - Ectocervix
Cervix - Endocervix
Colon - Sigmoid
Colon - Transverse
Esophagus - Gastroesophageal Junction
Esophagus - Mucosa
Esophagus - Muscularis
Fallopian Tube
Heart - Atrial Appendage
Heart - Left Ventricle
Kidney - Cortex
Kidney - Medulla
Liver
Lung
Minor Salivary Gland
Muscle - Skeletal
Nerve - Tibial
Ovary
Pancreas
Pituitary
Prostate
Skin - Not Sun Exposed (Suprapubic)
Skin - Sun Exposed (Lower leg)
Small Intestine - Terminal Ileum
Spleen
Stomach
Testis
Thyroid
Uterus
Vagina
Whole Blood
0
3.0
Log10(TPM+1)

Figure 15